Bulletin of Mathematical Biology Vol. 55, No. 4, pp. 745–780, 1993.
Printed in Great Britain.

0092-8240/93$6.00 + 0.00
Pergamon Press Ltd
Society for Mathematical Biology

IMMUNE NETWORK BEHAVIOR—I. FROM STATIONARY STATES TO LIMIT CYCLE OSCILLATIONS

■ ROB J. DE BOER†
Theoretical Biology,
Utrecht University,
Padualaan 8,
3584 CH Utrecht,
The Netherlands
(*E.mail:deboer@cc.ruu.nl*)

■ ALAN S. PERELSON
†Theoretical Division,
Los Alamos National Laboratory,
Los Alamos, NM 87545, U.S.A.
(*E.mail:asp@receptor.lanl.gov*)

■ IOANNIS G. KEVREKIDIS
Department of Chemical Engineering,
Princeton University,
Princeton, NJ 08544, U.S.A.
(*E.mail:yannis@arnold.princeton.edu*)

We develop a model for the idiotypic interaction between two B cell clones. This model takes into account B cell proliferation, B cell maturation, antibody production, the formation and subsequent elimination of antibody–antibody complexes and recirculation of antibodies between the spleen and the blood. Here we investigate, by means of stability and bifurcation analysis, how each of the processes influences the model's behavior. After appropriate non-dimensionalization, the model consists of eight ordinary differential equations and a number of parameters. We estimate the parameters from experimental sources. Using a coordinate system that exploits the pairwise symmetry of the interactions between two clones, we analyse two simplified forms of the model and obtain bifurcation diagrams showing how their five equilibrium states are related. We show that the so-called immune states lose stability if B cell and antibody concentrations change on different time scales. Additionally, we derive the structure of stable and unstable manifolds of saddle-type equilibria, pinpoint their (global) bifurcations and show that these bifurcations play a crucial role in determining the parameter regimes in which the model exhibits oscillatory behavior.

1. Introduction. Jerne (1974) postulated that the immune system functions as a network based upon idiotypic interactions among antibodies, B cells and T cells. In order to evaluate the role of network interactions in the operation of the immune system a number of models have been developed (see Perelson,

1988, 1989; Varela and Coutinho 1991, and De Boer *et al.*, 1992a for recent reviews). In this study we formulate a series of increasingly realistic models of the smallest B cell network possible, that is, one that only involves interactions between an idiotype and its anti-idiotype.

The main motivation for undertaking this study is that in previous work by De Boer and Hogeweg (1989b), De Boer *et al.* (1990), Perelson (1989) and Stewart and Varela (1989, 1990) fluctuations were found to be the predominant mode of dynamical behavior in network models that take into account both B cells and antibody. The fluctuations were either truly periodic or chaotic. Although the models had multiple steady states, for the parameter values thought to characterize immune networks these steady states were not stable. Analysis of the dynamic behavior in these models indicated that the fluctuations were due to the existence of two time scales, one determined by the B cell lifetime and the other by the antibody lifetime in the serum. Experimental data suggest that idiotype concentrations may indeed fluctuate periodically or chaotically on a time scale of two cycles per month (Lundkvist *et al.*, 1989; Varela *et al.*, 1991).

These results cast doubt on our earlier work (De Boer, 1988; De Boer and Hogeweg, 1989a; Weisbuch *et al.*, 1990), as well as that of others (cf. Hoffmann, 1975; Richter, 1975, 1978; Segel and Perelson, 1988) studying somewhat simplified models lacking the distinction between B cells and antibody. The behavior of these simplified models is dominated by a number of stable steady states. The presence of multiple attractors allowed us to interpret the model's behavior in terms of "virgin", "immune" and "suppressed" states. By switching from a virgin state, in which the B cells are inactive, to an immune state the models can account for the phenomenon of immunological memory. Furthermore, the existence of suppressed states could account for the phenomenon of immunological tolerance. This explanation of immunity and tolerance seems to be absent from models exhibiting large sustained oscillations in cell population sizes.

This paper will reconsider the question of whether the predominant mode of behavior of an immune system regulated by idiotypic network interactions is expected to be chaotic/oscillatory or stationary. In order to make the model realistic we consider two additional processes, and hence two new time scales. First, we incorporate a maturation period to account for the time-lag involved in B cell differentiation. We implement this as the "gearing up" process introduced by Segel and Perelson (1989). Second, as in Perelson and Weisbuch (1992) we examine a two-compartment model of the immune system. Note that these two complications are not required for the apparently chaotic behavior of the model, but do change the parameter regimes in which such behavior is observed.

The gearing up process models the time-dependent aspects of antibody

production. This involves a time lag associated with the differentiation of small stimulated B cells to the large lymphocyte and plasma cell states that are characteristic of antibody secreting cells. The time scale of such a gearing up process is of the order of several days. Using the method of Segel and Perelson (1989) we construct a first-order differential equation to describe gearing up. Other authors, e.g. Dibrov *et al.* (1977) and Fowler (1981), explicitly introduce a time delay τ such that the antibody production at time t depends on the B cell population, and its degree of stimulation, at a time $t-\tau$ in the past. The slow time scale that is introduced by incorporating the gearing up process will be shown to be destabilizing for the steady states.

Splitting the model into two compartments composed of the spleen and the bloodstream introduces a new time scale, the antibody residence time in the spleen (Perelson and Weisbuch, 1992). The spleen seems to be one of the primary lymphoid organs involved in idiotypic network interactions. Evidence for this includes the fact that animals raised in a germ-free environment have atrophic lymph nodes and are depleted of lymphocytes, whereas the spleen has roughly the same percentage of activated lymphocytes as in conventionally reared animals (Hooijkaas *et al.*, 1984; Pereira *et al.*, 1986). This activity is thought to be due to idiotypic interactions among components of the immune system. In the two-compartment model presented below, the residence time in the spleen becomes the most relevant time scale for the lifetime of antibody. Our calculations confirm the results of Perelson and Weisbuch (1992) that both long and short residence times in the spleen have destabilizing effects, and that stable equilibria are found for intermediate values of this residence time.

Responses to foreign antigens generally occur in lymph nodes. Thus, in modeling responses to foreign antigens one should include the set of lymph nodes as a compartment. Formally, the compartment model we introduce for the spleen can be used to model interactions in lymph nodes. Parameters such as the volume and flow rate (or, in general, the residence time distribution) would, however, have to be chosen differently.

2. The Two Compartment AB Model with Gearing Up. We have previously developed and studied a series of models for idiotypic B cell activation (De Boer *et al.*, 1990). The models differ in the specification of the activation process. In the simplest model we only consider B cells and ignore the fact that activation involves antibody molecules. In the "intermediate models" we incorporate antibodies but use a phenomenological description of the activation process involving antibody cross-linking. In our most detailed models we have considered the chemical reactions involved in receptor binding and cross-linking. We have called these models the B models (for B cell), the AB models (for antibody B cell) and the ABC models (for antibody B cell chemistry), respectively. In this paper we develop a more complete version of the AB

model, called the CABG model (for compartmental AB model with gearing up), which incorporates the time-lag involved in B cell differentiation and which distinguishes between a spleen compartment and a peripheral compartment. For reasons of simplicity and better understanding of the results, we will also study our previous models, which we here call the B model and the basic AB model.

In the CABG model we consider B cells localized in the spleen. These cells may become activated by interacting with an anti-idiotypic antibody, upon which they proliferate and differentiate into antibody secreting cells. This maturation process takes a few days. The free antibody, produced by differentiated activated B cells, activates anti-idiotypic B cells, leaves the spleen compartment due to fluid flow through the organ and reacts chemically with anti-idiotypic antibodies in either the spleen or the circulation to form complexes. These complexes, which are analogous to antigen–antibody complexes, are known to be removed from the system, for example by phagocytic cells such as macrophages. The rate of complex removal will turn out to be one of the crucial parameters of the model.

The CABG model, as well as some simplified versions of the model that we study, is derived from a combination of several previous models. We use the log bell-shaped activation function (see Fig. 1) that has been proposed as a phenomenological equation for the cross-linking process (Perelson and DeLisi, 1980; De Boer, 1988; De Boer *et al.*, 1990; Weisbuch *et al.*, 1990; De Boer and Perelson, 1991). The AB models make a distinction between B cells and the antibody along the lines of several earlier models (Varela *et al.*, 1988; De Boer and Hogeweg, 1989b; De Boer *et al.*, 1990; Perelson, 1989; De Boer and Perelson, 1991). The models incorporate the gearing up function proposed by Segel and Perelson (1989). The two-compartment model of the immune system, one compartment being the spleen and the other the bloodstream and fluids in which antibodies reside, is the one proposed by Perelson and Weisbuch (1992). For a more detailed explanation of these models we refer to these earlier publications.

We assume that all of the B cells of interest are localized in the spleen, whereas the antibody secreted by these cells enters the bloodstream. As a first approximation, we will treat both compartments as well-stirred and allow fluid flow at a rate q between compartments. For the spleen, which is a rather solid organ, this approximation need not be correct and is used for reasons of simplification. Because B cells generally need to interact with helper T cells and antigen presenting cells, both of which are present in high concentrations in the spleen, we feel that localizing the responding B cells to the spleen is more realistic than having B cells in both compartments. Let V_s be the volume available to antibodies in the spleen, let V_p be the available volume in the periphery, i.e. outside of the spleen, and let $v = V_s/V_p$ be the volume ratio. Thus,

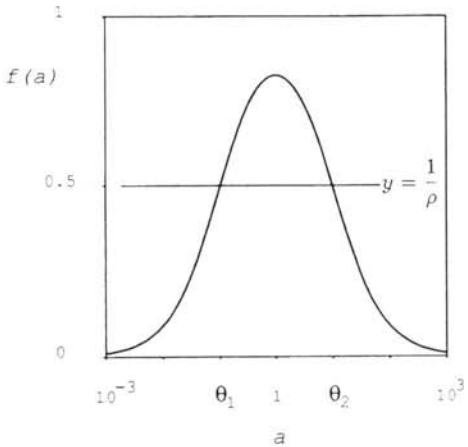

Figure 1. Graph of the bell-shaped proliferation function, $f(a)$, given by Equation (1) vs the field a. Equilibria involving proliferation, i.e. the immune and suppressed state, are located close the intersections of $f(a)$ with the line $y = 1/\rho$ (see text).

if q is expressed as a volume flow rate with units of volume/time, the average residence time of a molecule in the spleen is $\tau = V_s/q$, while the average residence time outside the organ is $V_p/q = \tau/v$.

In the AB models we use a phenomenological bell-shaped activation function:

$$f(a) = \frac{a}{\theta_1 + a} \frac{\theta_2}{\theta_2 + a}, \tag{1}$$

where $\theta_2 \gg \theta_1$, see Fig. 1. The use of a bell-shaped activation function can be justified on the basis of empirical dose–response curves for antibody production (cf. Celada, 1971) or on the basis of a more microscopic theory in which one assumes that activation is proportional to the fraction of cell surface immunoglobulin receptors cross-linked (cf. Perelson, 1984). We assume that B cell proliferation is governed by the same activation function. Segel and Perelson (1991) show that on the time scale of interest in immunological processes, hours to days, the chemical reactions involved in receptor binding and cross-linking can be considered to be fast and the ABC model can formally be approximated by the basic AB model under conditions where the amount of antibody per B cell is large so that antibody depletion due to cell binding can be ignored.

The function $f(a)$ is composed of two factors. The first factor increases from 0 to 1, reaching its half-maximal value at θ_1, the second factor decreases from 1 to 0, reaching its half-maximal value at θ_2. For $\theta_2 \gg \theta_1$, the maximum

$\theta_2/(\sqrt{\theta_1}+\sqrt{\theta_2})^2$ is approximately one. This maximum is attained at $a=\sqrt{\theta_1\theta_2}$.

We write for the two B cell populations inside the spleen:

$$\frac{db_1}{dt} = m + b_1(pf(a_2) - d_B), \tag{2a}$$

$$\frac{db_2}{dt} = m + b_2(pf(a_1) - d_B). \tag{2b}$$

Here m is a source term corresponding to the generation of new B cells in the bone marrow that then make their way to the spleen. B cells have a finite lifespan; d_B is the *per capita* death rate of B cells. The *per capita* rate of proliferation of stimulated B cells is p. The function $f(a)$ multiplying p can be viewed as representing the fraction of B cells stimulated to proliferate. Alternatively, one can take the view that all cells proliferate at the rate $pf(a)$.

The change in antibody concentrations in the spleen is described by:

$$\frac{da_1}{dt} = sG_1b_1 - d_Aa_1 - d_Cv^2Ka_1a_2 - (a_1 - \hat{a}_1)/\tau, \tag{3a}$$

$$\frac{da_2}{dt} = sG_2b_2 - d_Aa_2 - d_Cv^2Ka_1a_2 - (a_2 - \hat{a}_2)/\tau. \tag{3b}$$

B cells when stimulated by anti-idiotypic antibody are assumed to secrete antibodies at a *per capita* rate $sG(t)$, where s is a parameter and $G(t)$ the gearing up variable. We have assumed the rate at which antibodies are produced is a function of time so as to model the differentiation of small B cells into antibody secreting cells. Antibody has a natural rate of turnover d_A. Antibody can also be eliminated by binding to anti-idiotypic antibody to form a complex, C, which is then assumed to be eliminated (by macrophages and other phagocytic cells) at a rate d_C. Because complex formation is a chemical process that should occur on a time-scale of seconds to minutes, we have assumed that the concentration of the complex is that at chemical equilibrium. Thus, we assume $C=v^2Ka_1a_2$, where v is the valence of the antibody and K is the affinity of the idiotype for anti-idiotypic antibodies.

The last term, $-(a_1-\hat{a}_1)/\tau$, takes into account the loss of antibodies from the spleen and the supply of antibodies from the blood. If the concentration of antibody in the spleen is a_1 and fluid leaves the spleen at a volume flow rate q, then qa_1 moles of antibody leave the spleen per unit time. The inverse residence time is $\tau^{-1}=q/V_s$, where V_s is the spleen volume. The loss of antibody per unit time from a volume V_s then reduces the antibody concentration at a rate $-qa_1/V_s=-a_1/\tau$. Similarly, when antibody at a concentration $\hat{a}_1$ in the

blood enters the spleen via fluid flow at rate q, it increases the concentration of antibody in the spleen at rate $q\hat{a}_1/V_s$.

The change in the antibody concentrations outside the spleen is described by:

$$\frac{d\hat{a}_1}{dt} = v(a_1 - \hat{a}_1)/\tau - d_A\hat{a}_1 - d_C v^2 K\hat{a}_1\hat{a}_2, \tag{4a}$$

$$\frac{d\hat{a}_2}{dt} = v(a_2 - \hat{a}_2)/\tau - d_A\hat{a}_2 - d_C v^2 K\hat{a}_1\hat{a}_2. \tag{4b}$$

Because the external compartment has volume V_p, the antibody concentrations $\hat{a}_i$, $i=1, 2$, change at the rate $qa_i/V_p = va_i/\tau$ due to inflow from the spleen and at the rate $-q\hat{a}_i/V_p$ via outflow from this compartment. The other two terms account for the spontaneous decay of antibodies and for their loss via complex formation, respectively.

The rate of production of antibodies by B cells is dependent upon the gearing up process:

$$\frac{dG_1}{dt} = g(f(a_2) - G_1), \tag{5a}$$

$$\frac{dG_2}{dt} = g(f(a_1) - G_2). \tag{5b}$$

We introduce a separate gearing up function for each clone so that $G_i(t)$ can be interpreted as the proportion of antibody-producing B cells of type i. Following Segel and Perelson (1989), we construct $G_i(t)$ as the solution of the first-order differential equation (5), where g is a constant that determines the characteristic time for gearing up. At $t=0$ we set $G_i(0)=0$ so that there is no initial secretion. When a clone, say clone 1, becomes activated, $f(a_2)$ increases from 0 to a positive value and $G_1(t)$ increases. If a_2 were constant, $G_1(t)$ would increase towards $G_1 = f(a_2)$. However, as a_2 changes in time $G_1(t)$ follows with a lag. Formally, $G_1(t) = ge^{-gt}\int_0^t f(a_2(t'))e^{gt'}dt'$.

3. Parameter Estimates. First we estimate the volumes of the two compartments. In humans the spleen is approximately 0.5% of the total body weight (Weiss, 1972). For a 70 kg human a normal spleen would therefore be 350 g. Assuming the density of tissues to be 1 g/ml, this corresponds to 350 ml. Only a minor part of this will be extracellular fluid, however. We estimate this to be

1% or 3.5 ml. The amount of blood is estimated to be 75 ml per kg of body weight (Strand, 1978). For a 70 kg human this amounts to a total blood volume of 5250 ml. This, however, consists of both cells and plasma fluid. The plasma volume is about 44 ml per kg of body weight (Strand, 1978). The total volume of plasma in a 70 kg body is, therefore, estimated to be 3080 ml. Thus, the ratio of the two volumes $v = 3.5/3080 \simeq 10^{-3}$. Some antibody could also leak out of the circulation into the tissue spaces but that generally only happens at sites of inflammation, and hence should not significantly change our rough estimate of v.

A lower limit for the residence time of fluid in the spleen can be estimated from the rate at which blood flows through the organ. The total daily human cardiac output is about 6.0 l/min or 8640 l/day (Landis and Pappenheimer, 1962). Approximately 3% of this, i.e. 2.6×10^5 ml/day, goes through the spleen (Pabst, 1988). The average residence time, τ, of fluid in the spleen should therefore be $3.5 \text{ ml}/2.6 \times 10^5 \text{ ml/day} = 1.35 \times 10^{-5}$ day (or approximately 1 sec). Thus, an upper limit for the rate at which antibody leaves the spleen, $1/\tau$, is $7.4 \times 10^4 \text{ day}^{-1}$. The actual rate is probably considerably lower. Before entering the blood stream antibodies must move through the tissue and lymph, where they have the opportunity to bind Fc receptors on cells. The binding to cells will substantially slow the movement of antibodies from their site of production to the blood. We know of no direct measurements of antibody residence times. There is no direct connection between the splenic artery and vein. However, the average residence time of cells brought into the spleen is thought to be several hours (Sprent, 1989).

Antibody concentrations are typically measured in μg/ml. One fully activated B cell can produce 10^4 molecules per sec. Per day, i.e. per 86,400 sec, this corresponds to $8.64 \times 10^8/6 \times 10^{23} = 1.44 \times 10^{-15}$ moles/cell/day. Using a molecular weight of 900,000 for IgM this is $1.44 \times 10^{-15} \times 9 \times 10^5 = 1.3 \times 10^{-9}$ g/cell/day. To transform this into a concentration we must multiply by the concentration of antibody producing cells. Here we shall measure B concentration in units of cells per spleen and hence we shall normalize the secretion rate by the volume of the spleen, i.e. the volume in which the antibodies are diluted. In μg per 3.5 ml volume of the spleen the rate of antibody production per cell per unit volume is $s = 1.3 \times 10^{-3}$ μg/cell/day/3.5 ml $= 3.7 \times 10^{-4}$ μg cell/day/ml.

A high affinity IgM interaction maximally corresponds to an equilibrium constant $K = 10^6$ l/mol. For a molecular weight of 900,000 this translates into $10^6/900{,}000 \simeq 1$ l/g or $K = 10^{-3}$ ml/μg. For IgM antibody the valence is $v = 10$. Antibodies are typically long-lived. Due to the lack of data we have to make a quite arbitrary choice. We assume that in the absence of clearance by complex formation, antibodies live 10 times longer than B cells. This corresponds to a lifetime of 20 days, i.e. to $d_A = 0.05$ per day. Con-

versely, we assume that antibody complexes are quickly removed. Davies *et al.* (1990) studied the formation and clearance of immune complexes and showed that in their system the half-life is of the order 10 min. We opted for a somewhat longer half-life. Modeling clearance of antibody–antibody complexes as a first-order process we choose $d_C = 10$ per day, i.e. a lifetime of the order 2 hr.

In our model we assume that all idiotypically activated B cells reside in the spleen. The bone marrow produces 10^{12} B cells per day. Because of cell division at the pre-B cell stage, we estimate that each clone will be approximately 10 cells. (Thus the 10^{12} cells per day would correspond to roughly 10^{11} different specificities.) Since most cells that leave the bone marrow home to the spleen, this corresponds to $m = 10$ cells per day for the entire spleen. If multiple clones express the idiotype then m would be higher (see Discussion). B cells have a lifetime of 1–2 days: $d_B = 0.5$ per day. In the absence of stimulation, $f(a) = 0$, we will have $m/d_B = 20$ B cells per spleen per specificity. Further, stimulated B cells divide about every 16 hr, i.e. $p = 1$ per day. The gearing up parameter, $g = 0.2$ per day, sets a time scale of antibody production of about 5 days.

In an attempt to estimate θ_1 and θ_2 we use previous results showing that the maximum of the cross-linking curve is located around $(vK)^{-1}$, where v is the valence of the antibody. For bivalent antibodies the maximum is exactly at $(vK)^{-1}$ (Perelson and DeLisi, 1980), whereas for higher valence antibodies it is displaced somewhat to lower values (Perelson, 1981). For IgM antibodies, i.e. $v = 10$, with an affinity $K = 10^{-3}$ ml/μg, maximum cross-linking is expected at an IgM concentration of 100 μg/ml (i.e. approximately 10^{-5} mol/l). The lower threshold, θ_1, should be at least one and possibly several orders of magnitude lower than this, e.g. $\theta_1 = 10$ μg/ml. The upper threshold, θ_2, should be one to several orders of magnitude higher than this, e.g. $\theta_2 = 10^3$ μg/ml.

4. Nondimensional CABG Model. We non-dimensionalize the CABG model by choosing a time scale based upon B cell lifetime, i.e. $T = td_B$. Further, let α be the typical concentration of antibody that gives rise to maximal cross-linking, i.e. $\alpha = (vK)^{-1}$. Then, let β be the B cell population that, when fully activated, can produced a steady-state antibody concentration of α μg/ml. Since, under these conditions, $dA/dt = s\beta - d_A\alpha = 0$, we obtain a dimensionless scaling factor $\beta = \alpha d_A/s$. We have seen above that $\alpha \simeq 100$ μg/ml and hence, $\beta \simeq 1.35 \times 10^4$. Further, let θ be the half width of the activation function when plotted vs the logarithm of the antibody concentration. Since the activation curve is symmetric around its maximum $A = 1$, where $A = a/\alpha$, when plotted on a logarithmic scale, $\theta = \theta_2/\alpha$ and $\theta^{-1} = \theta_1/\alpha$. Then the model simplifies into:

$$f(A)=\frac{A}{\theta^{-1}+A}\frac{\theta}{\theta+A}, \tag{6}$$

$$\frac{dB_1}{dT}=\sigma+B_1(\rho f(A_2)-1), \tag{7a}$$

$$\frac{dB_2}{dT}=\sigma+B_2(\rho f(A_1)-1), \tag{7b}$$

$$\frac{dA_1}{dT}=\delta(B_1G_1-A_1)-\mu A_1A_2-\lambda(A_1-\hat{A}_1), \tag{8a}$$

$$\frac{dA_2}{dT}=\delta(B_2G_2-A_2)-\mu A_1A_2-\lambda(A_2-\hat{A}_2), \tag{8b}$$

$$\frac{d\hat{A}_1}{dT}=\nu\lambda(A_1-\hat{A}_1)-\delta\hat{A}_1-\mu\hat{A}_1\hat{A}_2, \tag{9a}$$

$$\frac{d\hat{A}_2}{dT}=\nu\lambda(A_2-\hat{A}_2)-\delta\hat{A}_2-\mu\hat{A}_1\hat{A}_2, \tag{9b}$$

$$\frac{dG_1}{dT}=\gamma(f(A_2)-G_1), \tag{10a}$$

$$\frac{dG_2}{dT}=\gamma(f(A_1)-G_2), \tag{10b}$$

where $A_i=a_i/\alpha$, $\hat{A}_i=\hat{a}_i/\alpha$, $B_i=b_i/\beta$, $\delta=d_A/d_B$, $\sigma=mvKs/(d_Ad_B)$, $\rho=p/d_B$, $\mu=vd_C/d_B$, $\lambda=1/(\tau d_B)$, $\gamma=g/d_B$, $\alpha=(vK)^{-1}$, $\beta=d_A/(svK)$.

Based upon the parameter values derived above, we estimate $\theta=10$, $\delta=0.1$, $\sigma=1.48\times10^{-3}$, $\rho=2$, $\mu=200$, $\nu=10^{-3}$, $\lambda\leqslant1.5\times10^5$ and $\gamma=0.4$. Note that changing the affinity K of the idiotypic interaction only affects σ and the scales used to measure antibody and B cells. Thus, for $\sigma=0$, the model behavior becomes independent of affinity.

The CABG model, Equations (6)–(10), consists of eight differential equations and contains eight non-dimensional parameters. In order to understand the behavior of the model we will first examine two simpler models derived from the full model by letting certain parameters approach either zero or infinity. Further, we will exploit the inherent symmetry of the model with respect to clones 1 and 2 by using a new coordinate system. In this paper we describe the basic properties of the steady states and the dynamic behavior of the simplified models. In a second paper (De Boer *et al.*, 1993), Part II, we will build on the results obtained here and study the detailed behavior of the full model.

5. The Basic AB Model. We have previously studied, via numerical methods, a simplified version of the CABG model with four equations and five parameters, which we now call the basic AB model (De Boer *et al.*, 1990). Here as a first step in the analysis of the full eight equation CABG model, we return to this model. The CABG model can be reduced to this basic AB model by setting $\lambda = 0$ and $\gamma \to \infty$, and choosing $\hat{A}_1(0) = \hat{A}_2(0) = 0$. This means that there is effectively only one compartment, i.e. the spleen, and no gearing up is required for antibody production. For these parameter values $\hat{A}_1(t) = \hat{A}_2(t) = 0$. Further, $G_1 \to f(A_2)$ and $G_2 \to f(A_1)$. Thus, the basic AB model is composed of Equation (6) for $f(A)$, Equation (7a), (b) for B_1 and B_2, and

$$\frac{dA_1}{dT} = \delta(B_1 f(A_2) - A_1) - \mu A_1 A_2, \tag{11a}$$

$$\frac{dA_2}{dT} = \delta(B_2 f(A_1) - A_2) - \mu A_1 A_2. \tag{11b}$$

In order to pinpoint the symmetry of this model more closely, we define another coordinate system. First, since the populations expand several orders of magnitude we change to logarithmic variables $b^* \equiv \ln B$, $a^* \equiv \ln A$. In logarithmic coordinates we obtain for the B cells:

$$\frac{db_1^*}{dT} = \sigma e^{-b_1^*} + \rho f(e^{a_2^*}) - 1, \tag{12a}$$

$$\frac{db_2^*}{dT} = \sigma e^{-b_2^*} + \rho f(e^{a_1^*}) - 1, \tag{12b}$$

and for the antibodies:

$$\frac{da_1^*}{dT} = \delta(f(e^{a_2^*}) e^{b_1^* - a_1^*} - 1) - \mu e^{a_2^*}, \tag{13a}$$

$$\frac{da_2^*}{dT} = \delta(f(e^{a_1^*}) e^{b_2^* - a_2^*} - 1) - \mu e^{a_1^*}, \tag{13b}$$

where

$$f(e^a) = \frac{e^a}{\theta^{-1} + e^a} \frac{\theta}{\theta + e^a}. \tag{14}$$

Second we define a new coordinate system, which we call the symmetric logarithmic (SL) coordinate system. The SL coordinate system exploits the symmetry of the model and will prove to be advantageous for making Poincaré sections. Thus, we define $b_d \equiv b_1^* - b_2^*$, $a_d \equiv a_1^* - a_2^*$, i.e. the difference between

the log concentrations (and hence, the log of the quotient of the concentrations), and $b_s \equiv b_1^* + b_2^*$ and $a_s \equiv a_1^* + a_2^*$, i.e. the sum of the log concentrations (and hence, the log of the product of the concentrations). Thus, $b_d = 0$ whenever $b_1^* = b_2^*$ and $a_d = 0$ whenever $a_1^* = a_2^*$. In the SL coordinate system we obtain for the B cells:

$$\frac{db_d}{dT} = \sigma(e^{-b_1^*} - e^{-b_2^*}) - \rho(f(e^{a_1^*}) - f(e^{a_2^*})), \tag{15a}$$

$$\frac{db_s}{dT} = \sigma(e^{-b_1^*} + e^{-b_2^*}) + \rho(f(e^{a_1^*}) + f(e^{a_2^*})) - 2; \tag{15b}$$

and for the antibodies:

$$\frac{da_d}{dT} = \delta(f(e^{a_2^*})e^{b_1^* - a_1^*} - f(e^{a_1^*})e^{b_2^* - a_2^*}) - \mu(e^{a_2^*} - e^{a_1^*}), \tag{16a}$$

$$\frac{da_s}{dT} = \delta(f(e^{a_2^*})e^{b_1^* - a_1^*} + f(e^{a_1^*})e^{b_2^* - a_2^*} - 2) - \mu(e^{a_2^*} + e^{a_1^*}), \tag{16b}$$

where $b_1^* \equiv (b_d + b_s)/2$ and $b_2^* \equiv (b_s - b_d)/2$, and $a_1^* \equiv (a_d + a_s)/2$ and $a_2^* \equiv (a_s - a_d)/2$.

6. The B Model. We have previously proposed an even simpler model (De Boer, 1988; De Boer and Hogeweg, 1989a; De Boer *et al.*, 1990; Weisbuch *et al.*, 1990). We now call this model the B model (for B cell model). Although the B model does not make a distinction between antibody and B cells, the steady states of the B model are very similar to those of the AB models. The B model has the advantage in that its steady states can be obtained analytically and their stability is easily analysed. Understanding AB models is greatly facilitated by examining the steady states of the B model.

The B model has a similar log bell-shaped activation function:

$$f(b) = \frac{b}{\theta_1 + b}\frac{\theta_2}{\theta_2 + b}, \tag{17}$$

and very similar B cell equations:

$$\frac{db_1}{dt} = m + b_1(pf(b_2) - d_B), \tag{18a}$$

$$\frac{db_2}{dt} = m + b_2(pf(b_1) - d_B). \tag{18b}$$

Thus, in the B model we ignore antibodies and assume that B cells activate each other according to the phenomenological activation function $f(b)$.

We nondimensionalize the B model by a procedure similar to the one we used above for the AB model, i.e. we let $T = td_B$ and we scale B cells by $\beta = \sqrt{\theta_1 \theta_2}$, the maximum of $f(b)$. We obtain:

$$f(B) = \frac{B}{\theta^{-1} + B} \frac{\theta}{\theta + B}, \tag{19}$$

$$\frac{dB_1}{dT} = \sigma + B_1(\rho f(B_2) - 1), \tag{20a}$$

$$\frac{dB_2}{dT} = \sigma + B_2(\rho f(B_1) - 1), \tag{20b}$$

where $B_i = b_i/\beta$, $\sigma = m/(\beta d_B)$ and $\rho = p/d_B$. In our previous work we analysed this model for $m = 1$ cell per day, $p = 1$ per day, $d_B = 0.5$ per day, $\theta_1 = 10^2$ cells and $\theta_2 = 10^4$ cells. Using these parameter values we find $\beta = 10^3$, $\sigma = 0.002$, $\rho = 2$ and $\theta = 10$. For these parameters this model has three stable and two unstable equilibria (see Fig. 2a).

We also define the B model in the symmetric logarithmic (SL) coordinate system by changing to logarithmic variables, $b^* \equiv \ln B$, i.e.

$$\frac{db_1^*}{dT} = \sigma e^{-b_1^*} + \rho f(e^{b_2^*}) - 1, \tag{21a}$$

$$\frac{db_2^*}{dT} = \sigma e^{-b_2^*} + \rho f(e^{b_1^*}) - 1, \tag{21b}$$

and then defining $b_d \equiv b_1^* - b_2^*$ and $b_s \equiv b_1^* + b_2^*$. In this coordinate system the B model becomes:

$$\frac{db_d}{dT} = \sigma(e^{-b_1^*} - e^{-b_2^*}) - \rho(f(e^{b_1^*}) - f(e^{b_2^*})), \tag{22a}$$

$$\frac{db_s}{dT} = \sigma(e^{-b_1^*} + e^{-b_2^*}) + \rho(f(e^{b_1^*}) + f(e^{b_2^*})) - 2, \tag{22b}$$

where $b_1^* \equiv (b_d + b_s)/2$ and $b_2^* \equiv (b_s - b_d)/2$. The activation function becomes:

$$f(e^b) = \frac{e^b}{\theta^{-1} + e^b} \frac{\theta}{\theta + e^b}. \tag{23}$$

7. Classification of Steady States. In our previous work we established that the B and basic AB models have similar steady states (De Boer, 1988; De Boer and Hogeweg, 1989a; De Boer *et al.*, 1990; Weisbuch *et al.*, 1990; Perelson and

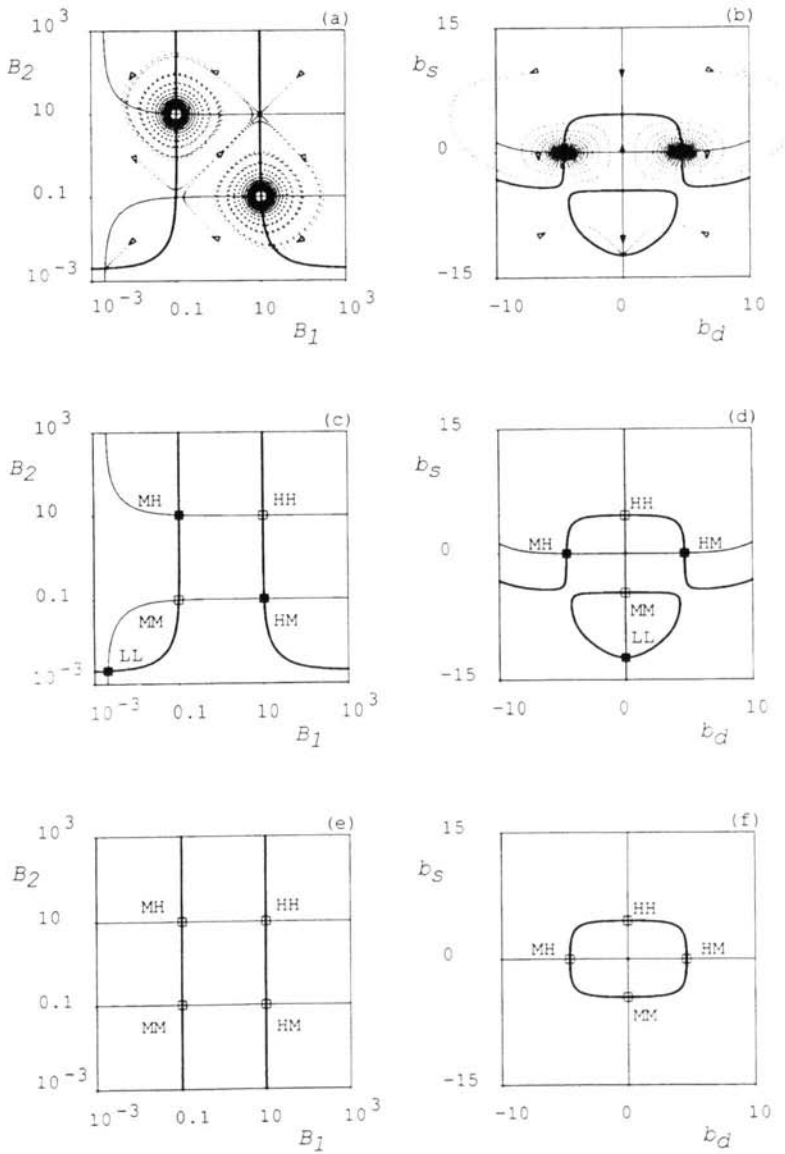

Figure 2. Trajectories, nullclines and steady states of the B model in the original and in the SL coordinate system. The heavy lines are the $B_2' = 0$ and $b_s' = 0$ nullclines, the light lines are the $B_1' = 0$ and $b_d' = 0$ nullclines. The boxes (□) denote equilibria: black means stable, open means unstable. Parameters: $\theta = 10$, $\rho = 2$, $\sigma = 0.002$. Panels (a), (c) and (e) are in the old coordinate system B_1 and B_2. Panels (b), (d) and (f) are in the SL coordinate system b_d and b_s. (a) and (b) Nullclines (lines) and trajectories (dots). (c) and (d) Nullclines and steady states. (e) and (f) Nullclines and steady states for $\sigma = 0$. The numerical methods for obtaining the figures are discussed in the appendix of the companion paper.

Weisbuch, 1992). First, there exist steady states that we call virgin states. A virgin state is symmetric, i.e. $b_1 = b_2$ or $b_d = 0$. In a virgin state the system may be considered to be at rest: B cell populations and/or antibody populations are small, too small to be able to evoke any significant proliferation. In terms of the model equations this means that $f(\cdot) \approx 0$, and hence that $b_i \approx m/d_B$, i.e. $B_i \approx \sigma$, and that $b_s = 2 \ln \sigma$ and $b_d = 0$.

Second we have described four activated steady states in which B cell populations are enlarged by proliferation, and for the AB models antibodies are being produced. In the activated states the contribution of the B cell source from the bone marrow, σ, is typically negligible because B cells are being renewed by continuous proliferation. In terms of the B cell Equations (7) and/or (20), and Fig. 1, such a proliferative equilibrium is reached when $f(h) \approx 1/\rho$, where the field, h, is either A_i [in Equation (7)] or B_i [in Equation (19)]†. Because the maximal rate of B cell proliferation must be greater than the rate of B cell death to obtain clonal expansion during an immune response, we assume that $\rho > 1$. Further, since $f(h)$ is a hump shaped function with $0 \leqslant f(h) < 1$ we typically find two equilibria for two different values of h. The first equilibrium, the immune state, corresponds to $h \approx \theta^{-1}$. To see this, note that for $h \approx \theta^{-1} \ll \theta$ the second factor in $f(h)$, $\theta/(\theta + h) \approx 1$. Thus, the bell-shaped function can be approximated by the first factor and we obtain:

$$f(h) \approx \frac{h}{\theta^{-1} + h} \approx \frac{1}{\rho}, \text{ hence } h \approx \frac{1}{\theta(\rho - 1)}. \tag{24a}$$

The state is called "immune" because the cells are proliferating and because increasing the degree of stimulation, h, will increase the rate of proliferation (Fig. 1).

The second equilibrium, the suppressed state, corresponds to $h \approx \theta$. For $h \approx \theta \gg \theta^{-1}$ the first factor is $f(h)$, $h/(\theta^{-1} + h) \approx 1$. Thus, the bell-shaped function can be approximated by the second factor and we obtain:

$$f(h) \approx \frac{\theta}{\theta + h} \approx \frac{1}{\rho}, \text{ hence } h \approx \theta(\rho - 1). \tag{24b}$$

Although the cells are proliferating, we call this a suppressed state because increasing the degree of stimulation, h, decreases the rate of proliferation (Fig. 1). For $\rho \approx 2$ the two solutions, Equations (24a) and (b), reduce to $h \approx \theta^{-1}$ and $h \approx \theta$, respectively. This provides the equilibrium values of B_i in the B model and of A_i in the basic AB model.

Since in equilibrium $G_i = f(a_i)$ we derive for both the CABG model and basic AB model the equilibrium values of B_i by solving Equations (11a) and (b):

$$\delta(B_1 f(A_2) - A_1) - \mu A_1 A_2 = 0, \tag{25a}$$

† For small positive values of σ the steady state is obtained when $f(h)$ is somewhat less than $1/\rho$.

$$\delta(B_2 f(A_1) - A_2) - \mu A_1 A_2 = 0. \tag{25b}$$

By Equations (24a) and (b), $f(A_1) \approx f(A_2) \approx 1/\rho$, in the activated equilibria. We thus obtain:

$$B_1 \approx \rho A_1 \left(1 + \frac{\mu}{\delta} A_2\right) \tag{26a}$$

and

$$B_2 \approx \rho A_2 \left(1 + \frac{\mu}{\delta} A_1\right), \tag{26b}$$

where A_1 and A_2 are given by Equations (24a) and (b). For $\mu = 0$ in the activated equilibria $B_1 = \rho A_1$ and $B_2 = \rho A_2$, i.e. B_i and A_i are proportional to each other. When B_i and A_i are proportional they need not be treated separately and our simplest B model would be sufficient. However, since we generally have $\mu \neq 0$, B cell and antibody populations are not proportional (see also De Boer and Perelson, 1991). A more thorough analysis of the steady states in the B and basic AB models will be given in Sections 8 and 9. Our goal here was simply to characterize them as virgin, immune or suppressed.

Since we have an immune and a suppressed equilibrium for each of the two clones we typically have four activated equilibria. In the activated equilibria clones proliferate and contain more cells than clones in the virgin state $B_1 \approx \sigma$. Clones in the virgin state are, therefore, called "L" for low, and clones in an activated state are either "M" for moderate (i.e. for θ^{-1}) or "H" for high (i.e. for θ). The model has two asymmetric equilibria in which one clone is immune and the other is suppressed (see Figs 2 and 3). Here one clone is "high" and the other is "moderate". We call these states "HM" and "MH". These asymmetric states have also been called "immune" states since the clone that is high can respond to antigen very efficiently. Further, in B models such immune states can be obtained by perturbing the virgin state with an antigen (cf. Weisbuch *et al.*, 1990). We shall also refer to these asymmetric states as immune states when no confusion with the state of a single clone will arise. Note that in an asymmetric equilibrium the high clone has a moderate field, i.e. is immune, and that the moderate clone has a high field, i.e. is suppressed. The model also has two symmetric equilibria in which both clones are immune or suppressed (see Figs 2 and 3). These are called the "HH" and "MM" states. Note that in the symmetric equilibria high level clones have high fields, i.e. are suppressed, and that moderate level clones have moderate fields, i.e. are immune. Thus, high or low levels do not correlate with the immune or suppressed state. To determine whether a clone will grow under the influence of further stimulation one must examine its field, not its population level.

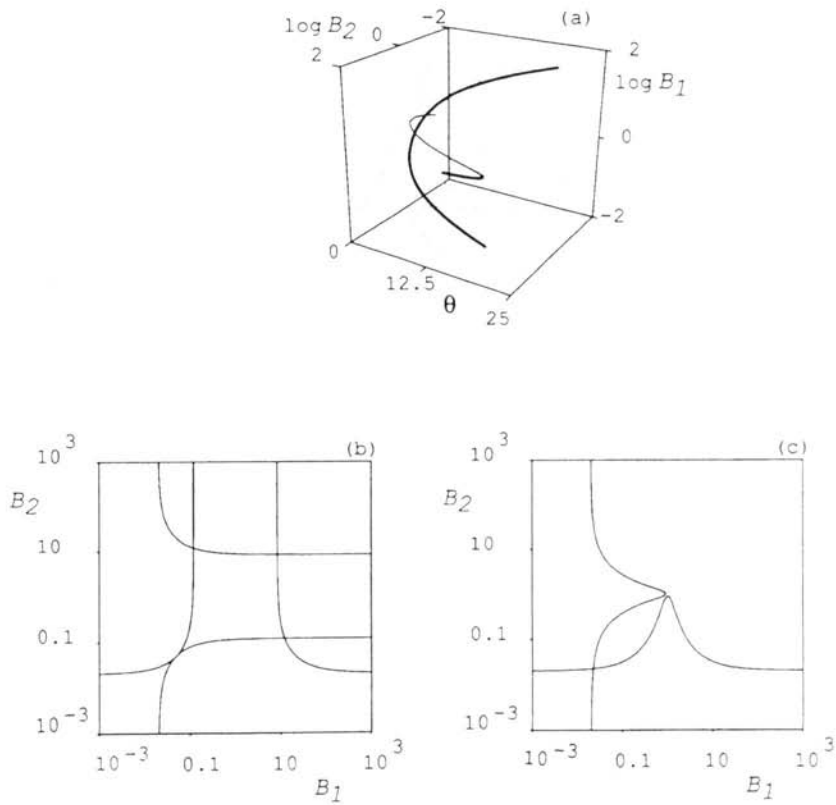

Figure 3. Bifurcation diagram and nullclines of the B model varying θ as a bifurcation parameter. Parameters: $\rho = 2$, $\sigma = 0.02$ (we have increased σ 10-fold to improve the graphical representation). Heavy lines denote stable steady states, light lines denote unstable steady states. The gray lines form the projections of the three-dimensional diagram onto each of the sides. (a) Bifurcation diagram for $0 \leq \theta \leq 25$. (b) Nullclines for parameter values close to the bifurcation point $\theta = 8.65$. (c) Nullclines for parameter values close to the two bifurcation points at $\theta \approx 2.33$.

In the SL coordinate system the four activated states can easily be recognized as states where one of the variables equals zero. In the symmetric HH and MM states $A_1 = A_2$ and/or $B_1 = B_2$, which can be recognized by $a_d = 0$ and/or $b_d = 0$. In the asymmetric states, HM and MH, the two fields, h_i, are of the order θ^{-1} and θ. Thus, $a_s \approx 0$ or $b_s \approx 0$, i.e. the sum of the logarithmic variables $a_s = a_1 + a_2$ or $b_s = b_1 + b_2$ is approximately $\ln \theta + \ln 1/\theta = 0$.

8. Stability and Bifurcation Analysis of the B Model.

8.1. *Steady states.* The precise values of the steady states of the B model can be determined analytically. Setting the left-hand sides of Equations (20a) and (b) to zero and substituting Equation (19) yields:

$$0=\sigma(\theta^{-1}+B_2)(\theta+B_2)+B_1[\rho B_2\theta-(\theta^{-1}+B_2)(\theta+B_2)], \tag{27a}$$

$$0=\sigma(\theta^{-1}+B_1)(\theta+B_1)+B_2[\rho B_1\theta-(\theta^{-1}+B_1)(\theta+B_1)]. \tag{27b}$$

Solving Equation (27a) for B_1 gives:

$$B_1=\frac{\sigma(\theta^{-1}+B_2)(\theta+B_2)}{(\theta^{-1}+B_2)(\theta+B_2)-\rho\theta B_2}. \tag{28}$$

Substituting Equation (28) into Equation (27b) and rearranging yields a fifth order polynomial in B_2 that can be factored into the product of a cubic and a quadratic polynomial. The roots of these polynomials give the five possible steady states. The cubic can be derived directly from Equations (27) in the following manner. Subtracting Equation (27b) from (27a) we see that $B_1=B_2\equiv B$ is a solution of the resulting equation. Substituting B for B_1 and B_2 into Equation (27a) or (27b) yields the cubic equation:

$$(\sigma-B)(\theta^{-1}+B)(\theta+B)+\rho\theta B^2=0,$$

or equivalently:

$$B^3+[\theta+\theta^{-1}-\sigma-\rho\theta]B^2+[1-\sigma(\theta+\theta^{-1})]B-\sigma=0. \tag{29}$$

From Descartes' rule of signs it follows that in order for Equation (29) to have three real positive roots, it is necessary that there be three sign changes. Thus, it is necessary that (i) the coefficient of B^2 be negative, i.e. $\theta+\theta^{-1}-\sigma-\rho\theta<0$; and (ii) the coefficient of B be positive, i.e. $\rho<[\theta+\theta^{-1}]^{-1}$. For our standard values, $\rho=2$, $\theta=10$ and $\sigma=0.002$, both of these conditions are met. However, with $\theta=10$, condition (ii) will not be met if $\sigma\geqslant 0.1$.

Solutions of Equation (29) yield the three possible symmetric steady states in which $B_1=B_2$. These are the states that we previously have called LL, MM and HH. For certain parameter values two of the real positive roots of Equation (29) will be equal and only two steady states will exist. The condition for the equality of roots is well known (cf. Abramowitz and Stegun, 1965) and not repeated here. However, we will see below in our numerical work that with $\sigma=0.02$ and $\rho=2$, this condition is met and the HH and MM states merge when $\theta=2.331$; the LL and MM states merge when $\theta=8.647$. From Equation (29) we can also see that the virgin state, LL, is not exactly at $B=\sigma$. Neglecting the quadratic and cubic terms in Equation (29) we see that a better approximation to the virgin state is $B=\sigma/(1-\sigma[\theta+\theta^{-1}])$.

Using Mathematica (Wolfram Research Inc.) to analyse the fifth-order polynomial that results when Equation (28) is substituted into Equation (27b), we find that the quadratic polynomial is:

$$[(\rho-1)\sigma\theta-(\sigma^2+1)-\sigma\theta^{-1}]B_2^2$$
$$+[(\rho-1)\sigma\theta^2+(\rho-1-\sigma^2)\theta+(\rho-2)\sigma-(\sigma^2+1)\theta^{-1}-\sigma\theta^{-2}]B_2$$
$$-(\sigma+\theta)(\sigma+\theta^{-1})=0. \tag{30}$$

The solutions of Equation (30) yield B_2 in the asymmetric steady states, HM and MH. B_1 in these steady states is then found from Equation (28).

From this analysis we see that there are at most three symmetric and two asymmetric steady states. By solving the cubic and quadratic equations (29) and (30) we can obtain the values of B_1 and B_2 for these steady states. We can also analyse the conditions under which these various steady states merge and disappear. For example, when the discriminant of the quadratic equation (30) is zero, its two real roots coincide. If the discriminant becomes negative there will be no asymmetric real solutions. Because the solutions to both the quadratic and cubic are algebraically complicated, we will study the properties of these steady states numerically.

8.2. *Stability of steady states.* From Equation (20) the stability of the steady states is governed by the eigenvalues of the following Jacobian matrix:

$$J=\begin{bmatrix} \rho f(\bar{B}_2)-1 & \rho\bar{B}_1 f'(\bar{B}_2) \\ \rho\bar{B}_2 f'(\bar{B}_1) & \rho f(\bar{B}_1)-1 \end{bmatrix}, \tag{31}$$

where $\bar{B}_i$ denotes the steady state value of $\bar{B}_i$, $i=1, 2$, and $f'(\bar{B}_i)$ denotes the value of the derivative of f evaluated at B_i. The eigenvalues are the solution of:

$$\lambda^2-\mathrm{tr}(J)\lambda+\det(J)=0 \tag{32}$$

where $\mathrm{tr}(J)$ and $\det(J)$ are the trace and the determinant of J, respectively. Let λ_1 and λ_2 be the two solutions of Equation (32). A stable steady state, which is characterized by both λ_1 and λ_2 with negative real parts, requires:

$$\mathrm{tr}(J)<0 \text{ and } \det(J)>0. \tag{33}$$

From Equation (20), at steady state $\rho f(\bar{B}_2)-1=-\sigma/\bar{B}_1$ and $\rho f(\bar{B}_1)-1=-\sigma/\bar{B}_2$. Hence:

$$\mathrm{tr}(J)=-\left(\frac{\sigma}{\bar{B}_1}+\frac{\sigma}{\bar{B}_2}\right)\leqslant 0, \tag{34a}$$

while

$$\det(J)=\frac{\sigma^2}{\bar{B}_1\bar{B}_2}-\rho^2\bar{B}_1\bar{B}_2 f'(\bar{B}_1)f'(\bar{B}_2). \tag{34b}$$

For either of the asymmetric steady states, HM and MH, $\bar{B}_1$ and $\bar{B}_2$ lie on

opposite sides of the bell shaped curve (see Fig. 1). Hence, $f'(\bar{B}_1)f'(\bar{B}_2)<0$ and $\det(J)\geqslant 0$. If there is a supply of cells from the bone marrow, i.e. if $\sigma>0$, then $\mathrm{tr}(J)<0$ and $\det(J)>0$ and we conclude that both asymmetric steady states are stable. In the singular case in which there is no supply of cells, $\sigma=0$, $\mathrm{tr}(J)=0$ and $\det(J)>0$ (assuming $\rho\neq 0$). Under these conditions Equation (32) implies $\lambda_i=\pm\sqrt{-\det(J)}$, $i=1, 2$, and the asymmetric steady states will be neutrally stable with purely imaginary eigenvalues.

A similar analysis applies to the symmetric steady states except now $f'(\bar{B}_1)f'(\bar{B}_2)>0$, since $\bar{B}_1=\bar{B}_2$, and $\det(J)$ may be positive or negative depending on the relative sizes of the two terms. In the virgin state, LL, $\bar{B}_i\simeq\sigma$ and the first term on the right-hand side of Equation (34b) is of the order 1, while the second term is of the order $\rho^2\sigma^2(\theta^{-1}/(\theta^{-1}+\sigma)^2)^2$. For our typical parameters, $\rho=2, \theta^{-1}=0.1, \sigma<\theta^{-1}$, the second term is small compared with 1, $\det(J)>0$, and we conclude that the virgin state is stable.

For the HH and MM state $\bar{B}_i$ is of the order θ and θ^{-1}, respectively. In these cases the first term on the right-hand side of Equation (34b) is smaller than the second and $\det(J)<0$. These states are thus unstable (saddle-type) with one positive and one negative eigenvalue. For any set of parameters precise calculations can be performed using the formulae given above. The results that we have given are typical for the parameter regime of interest but clearly changes in stability will occur with the relative sizes of the two terms in Equation (34b). Formally, we can conclude that for symmetric steady states in which $\bar{B}_1=\bar{B}_2=\bar{B}$:

$$\frac{\rho^2\bar{B}^4f'(\bar{B})^2}{\sigma^2}\begin{cases}<1\Rightarrow\det(J)>0\Rightarrow\text{stable}\\ >1\Rightarrow\det(J)<0\Rightarrow\text{unstable.}\end{cases}$$

8.3. *Nullclines.* In order to become familiar with the possible steady states of the model and with the SL coordinate system, we depict in Fig. 2 the nullclines of the B model in both the original and SL coordinate systems. (A nullcline is the locus of points along which a time derivative is zero.) The nullclines are drawn for $\sigma=0.002$ in Figs 2a–d, and for $\sigma=0$ in Figs 2e,f. the heavy lines are the $B_2'=0$ nullclines and the $b_s'=0$ nullclines, respectively (where $'$ denotes $\mathrm{d}(\cdot)/\mathrm{d}T$). Obviously, the nullclines of the two coordinate systems are different. The two systems only correspond at the intersections of the nullclines, i.e. at the steady states. As is shown by the intersections of the nullclines, the B model has five equilibrium states for these parameters. In Figs 2c–f stable equilibria are marked with a black square and unstable equilibria are marked with an open square. The trajectories, i.e. the dotted lines in Figs 2a and 1b, show how the LL, HM and MH states are attained from various initial conditions. In accordance with Equations (24a) and (24b), the

four activated states HM, MH, MM and HH are located around $B_i \approx \theta$ and/or $B_i \approx 1/\theta$, or around $b_d = 0$ and/or $b_s = 0$, respectively. The symmetric virgin state, LL, is located around $B_1 = B_2 = \sigma$ in the old coordinate system, and around $b_d = 0$ and $b_s = 2 \ln \sigma$ in the SL coordinate system.

For $\sigma = 0$, i.e. Figs 2e,f, the nullclines become straight lines in the original coordinate system and straight lines plus an ellipsoid in the SL coordinate system. The main difference is the loss of the LL state. Since the interpretation of nullclines in the SL system is not intuitively clear, we will not discuss them further. Additionally, all subsequent steady-state analysis will be presented in the original coordinate system. The SL coordinate system will be used to present the dynamic analysis.

8.4. *Saddle invariant manifolds and basins of attraction.* In order to understand the ultimate fate of transients (i.e. the basins of attraction of the stable solutions) and the birth and death of stable solutions in global bifurcations, we study the location and interactions of the invariant manifolds (stable and unstable) of the saddle-type equilibrium MM and HH states as the parameters vary.

The two asymmetric (immune) states, HM and MH, are sinks each with its own basin of attraction [see the trajectories spiraling inward in Figs. 2a,b]. The LL, MM and HH states are all located on the line of symmetry $B_1 = B_2$ or $b_d = 0$. On the line of symmetry the unstable MM state "separates" the LL and the HH state, see Figs 4a,b. In Fig. 4 we plot the stable and unstable manifolds (i.e. the insets and outsets) of the saddle-type MM and HH states. The one-dimensional stable manifold of the HH state lies on the line of symmetry. The HH state has a one-dimensional unstable manifold that is normal to the line of symmetry. For $\sigma > 0$ this manifold asymptotically approaches the stable immune states (e.g. Figs 2a,b, $\sigma = 0.002$); for $\sigma = 0$ it asymptotically connects with the unstable (saddle-type) MM state, coinciding with its one-dimensional stable manifold (see Fig. 3c,d). For $\sigma < 0$ this manifold approaches a negative virgin state $b_i = -\sigma$. (This is similar to Fig. 9c that arises in the study of the AB model.) It is not shown because $\sigma < 0$ or $b_i < 0$ is not meaningful. The global bifurcation at $\sigma = 0$, corresponding to the formation of this heteroclinic connection between the HH and the MM state, will prove to be very important for understanding the behavior of the AB models. (A heteroclinic connection is a connection between two distinct saddle-type equilibria). The one-dimensional unstable manifold of the MM state lies on the line of symmetry and approaches the LL state on one side and the HH state on the other side. At $\sigma = 0$ the one-dimensional stable manifold of the MM state is normal to the line of symmetry at the MM state, and coincides with the outset of HH state to form the heteroclinic connection shown in Figs 4c,d. The light lines in Figs 4c,d are the nullclines.

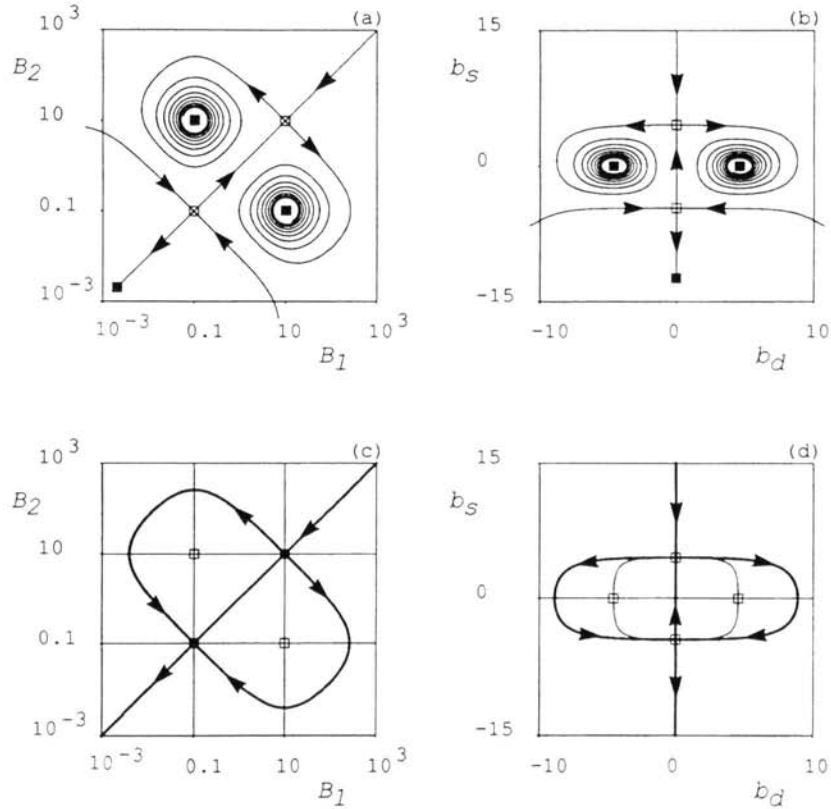

Figure 4. Stable and unstable invariant manifolds of the saddle-type MM and HH states in the B model. Parameters: $\theta = 10$ and $\rho = 2$. Panels (a) and (c) are in the original coordinate system B_1 and B_2. Panels (b) and (d) are in the SL coordinate system b_d and b_s. The boxes (□) denote equilibria: black means stable, open means unstable. The arrows indicate the dynamics on the invariant manifolds. (a, b) $\sigma = 0.002$; the light lines are the invariant manifolds of the MM and HH state. The unstable manifold of the HH state will spiral into the stable immune states. (c, d) $\sigma = 0$: the light lines are the nullclines. The heavy lines are the invariant manifolds. The unstable manifold of the HH state forms a heterocline connection with the MM state. Note that the LL state is absent because $\sigma = 0$.

8.5. *Bifurcations with respect to* θ. The relation between the five equilibria is analysed for $\sigma = 0.02$ in Fig. 3a, where we use θ as a bifurcation parameter. Here heavy lines denote stable steady states and light lines unstable equilibria. The two curves in Fig. 3a correspond to the solutions of the cubic and the quadratic polynomial studied in Equations (29) and (30). The solution corresponding to the symmetric states is an S-shaped curve with turning points at $\theta \approx 2.3$ and $\theta \approx 8.6$ [see Equation (29)]. For $0 < \theta < 2.3$ the only steady state is

the virgin state. As θ increases, the MM and HH states are born together in a saddle-node bifurcation at $\theta \approx 2.331$. Thus, three symmetric states (i.e. LL, MM, and HH) co-exist for $2.331 < \theta < 8.6$. The MM and the virgin LL states collide and disappear in a second saddle-node bifurcation at $\theta = 8.6$. The solution branch corresponding to the asymmetric states is parabolic with the turning point at $\theta \approx 2.338$ [see Equation (30)]. This turning point intersects the cubic solution for the symmetric states. At this point the two asymmetric immune states bifurcate from the symmetric HH state in a pitchfork bifurcation. This pitchfork bifurcation and the saddle-node bifurcation at $\theta \approx 2.331$, where the MM and HH states are born, visually appear as a single bifurcation point in Fig. 3a because they occur so close in parameter space.

These bifurcations are shown in terms of nullclines in Figs 3b,c. The nullclines corresponding to the saddle-node bifurcation where the virgin state disappears are shown in Fig. 3c. For $\theta = 8.6$ one can see the $b_1' = 0$ and $b_2' = 0$ nullclines barely touching in Fig. 3b. The reason for the loss of the virgin state is that with θ sufficiently large, the field generated by a low B cell population suffices for the initiation of proliferation. The nullclines around $\theta = 2.3$ are shown in Fig. 3c. Decreasing θ from its default value of 10, the distance between the immune and the suppressed states decreases. In Fig. 3c this is illustrated by the two nullclines just barely touching in the middle.

Summarizing, the B model for $\rho = 0.02$ has one steady state for $\theta < 2.3$. Then after two bifurcations at $\theta = 2.331$ and $\theta = 2.338$, five steady states for $2.34 < \theta < 8.6$ and three steady states for $\theta > 8.6$. The location of the last bifurcation point strongly depends on σ. The two bifurcation points are close together in Fig. 3 because we increased σ 10-fold above its default value. For lower values of σ the bifurcation diagram remains qualitatively the same, but the two bifurcation points are widely separated and would require a logarithmic θ axis to visualize them in one graph.

9. Analysis of the Basic AB Model.

9.1. *Steady states.* The steady states of the basic AB model, defined by Equations 6, 7a,b and 11a,b, can be analysed in a manner comparable to that of the B model. At steady state, Equations 7 and 11 become:

$$0 = \sigma + B_1(\rho f(A_2) - 1), \tag{35a}$$

$$0 = \sigma + B_2(\rho f(A_1) - 1), \tag{35b}$$

$$0 = \delta(B_1 f(A_2) - A_1) - \mu A_1 A_2 \tag{36a}$$

$$0 = \delta(B_2 f(A_1) - A_2) - \mu A_1 A_2 \tag{36b}$$

Hence, from (35) with $\sigma \neq 0$:

$$B_1 = \frac{\sigma}{1-\rho f(A_2)}, \tag{37a}$$

$$B_2 = \frac{\sigma}{1-\rho f(A_1)}. \tag{37b}$$

Equations (36) give, for $\delta \neq 0$:

$$B_1 = \frac{A_1(\mu A_2 + \delta)}{\delta f(A_2)}, \tag{38a}$$

$$B_2 = \frac{A_2(\mu A_1 + \delta)}{\delta f(A_1)}. \tag{38b}$$

Equating the right-hand sides of Equations (37a) and (38a), and the right-hand sides of Equations (37b) and (38b), we obtain:

$$\sigma\delta f(A_2) = A_1[1-\rho f(A_2)]\,[\mu A_2 + \delta], \tag{39a}$$

$$\sigma\delta f(A_1) = A_2[1-\rho f(A_1)]\,[\mu A_1 + \delta], \tag{39b}$$

equations whose solution give the steady state values of A_1 and A_2.

One class of solutions are the symmetric solutions with $A_1 = A_2 = A$. From Equation (39a), with $A_1 = A_2 = A$, and substituting Equation (6) for $f(A)$, one obtains after some algebraic simplification:

$$A[\mu\theta A^3 + (\mu + \delta\theta - \mu\theta^2(\rho-1))A^2 + (\mu\theta + \delta - \delta\theta^2(\rho-1))A + \delta\theta(1-\sigma\theta)] = 0. \tag{40}$$

One solution is $A = 0$. In this state both antibody populations are zero and we thus call this state ZZ (for zero–zero). The B cell populations, from Equation (35), are $B_1 = B_2 = \sigma$. Hence, the ZZ state is a virgin state in which no antibody is present to activate the network.

The other symmetric solutions are the real positive roots of the cubic given in brackets. Notice, that if $\sigma\theta < 1$, then the first and last term of the cubic are positive. If the two middle terms are both positive, then there are no sign changes and the cubic will have no real positive roots. However, if one or both of the middle terms is negative then there are two sign changes, and hence by Descartes' rule of signs the cubic has two or no real positive roots. For the parameters $\rho = 2$, $\theta = 10$, $\delta = 0.1$, $\mu = 20$ and $\sigma = 1.48 \times 10^{-3}$ this latter case applies and we expect two or no real positive solutions. In fact, for these parameters the constant term in the cubic is negligible compared to the other terms and the equation can be approximated by a quadratic with two real positive roots. These roots correspond to the HH and MM states of the B model. In this regime, i.e. when $\sigma\theta < 1$, the LL state is negative (cf. Fig. 5c).

Conversely, when $\sigma\theta > 1$ the last term of the cubic is negative. This means that we may have three sign changes. Then the cubic has one or three real solutions. The former case corresponds to the HH state (see Fig. 5c for $\sigma > 0.56$). The latter case corresponds to the LL, MM and HH states (see Fig. 5c for $\sigma < 0.56$).

Once the symmetric states are found, Equations (39a) and (39b) can be analysed for the asymmetric states. As in the case of the B model, a high-order polynomial is obtained by combining these equations. This equation can be factored, with one factor being Equation (40). The remaining factor is a sixth-order polynomial, which we have not attempted to analyse algebraically. Below, we study both the symmetric and asymmetric solutions numerically, focusing on the bifurcation behavior of the solutions in the parameter regimes of immunological interest.

9.2. *Comparison of the steady states of the basic AB model and the B model.* Graphically, the steady states of the AB model can be compared with those of the B model shown in Figs 2–4. First note that for $\sigma = 0$ the equilibria of the B cell equations [i.e. Equations (7a) and (7b)] depend only on the antibody concentrations. Thus, for $\sigma = 0$ we plot the B cell nullclines in the 2D phase space spanned by A_1 and A_2 (Fig. 5a). The nullclines are very similar and intersect in the same set of equilibria as those of the B model in Fig. 2e. Thus, the solutions correspond to $A_i = \theta$ or $A_i = \theta^{-1}$. For $\sigma = 0$, the stable virgin state is located at $B_1 = B_2 = A_1 = A_2 = 0$. This virgin state is not represented in Fig. 5a due to the logarithmic axis.

Varying θ as the principal bifurcation parameter, for $\sigma = 1.48 \times 10^{-3}$, we show in Fig. 5b that the HM, MH, HH and MM steady states are born around $\theta \approx 2.4$. The two curves in Fig. 5b are two parabolas corresponding to the symmetric and the asymmetric steady states, respectively. The parabola for the symmetric steady states is defined by the two real solutions of Equation (40). Thus, the same set of activated states is present in the B and the basic AB models. The main difference is the stability of the HM and the MH state. In the basic AB model these states are stable only in between two Hopf bifurcations located at $\theta \approx 3$ and $\theta \approx 16$, respectively (see the short heavy lines). The two bifurcations around $\theta = 2.4$ at which the four activated states are born are the same as those in the B model. Decreasing θ we first find a pitchfork bifurcation where the HH, MH and HM states unite. Here the HH state becomes stable until it undergoes the saddle-node bifurcation where the HH and MM states merge. In the basic AB model the values of θ for which the two bifurcations occur are even more close (i.e. the distance is less than 10^{-8}).

9.3. *Virgin states in the basic AB model.* We have seen above that the basic AB model has a new virgin ZZ state in which both antibody populations are

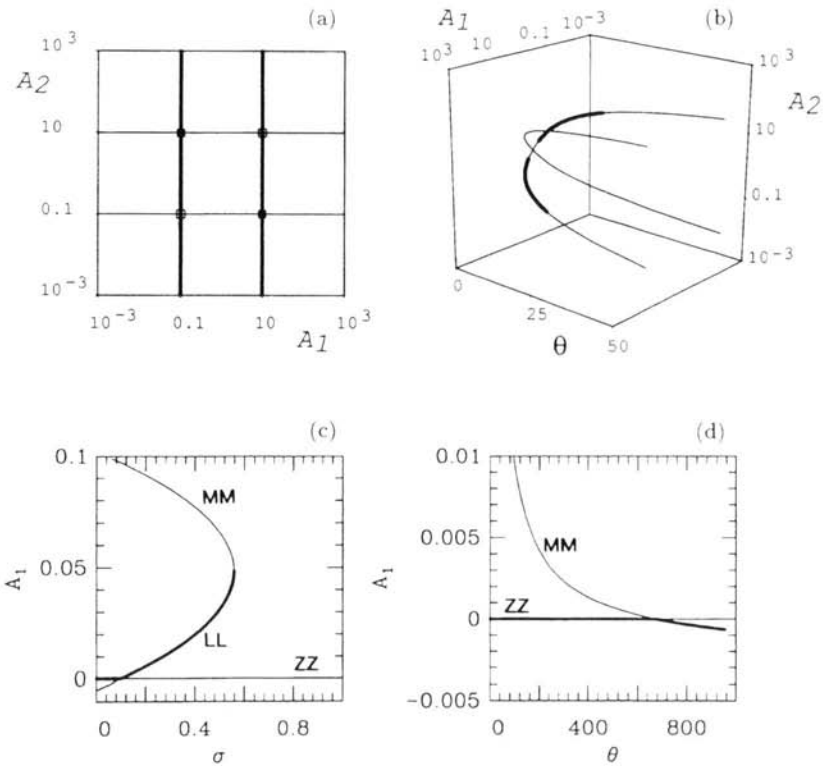

Figure 5. Equilibria of the basic AB model. Parameters: $\theta = 10$, $\rho = 2$, $\delta = 0.1$, $\mu = 20$. In panel (a) we show the B cell nullclines in the antibody phase space for $\sigma = 0$. The heavy and light lines denote the $B_2' = 0$ and $B_1' = 0$ nullclines, respectively. In panel (b) we show a bifurcation diagram of the basic AB model varying $0 \leqslant \theta \leqslant 50$ as a bifurcation parameter for $\sigma = 1.48 \times 10^{-3}$. The heavy lines denote stable states, light lines denote unstable states. The four equilibria are born around $\theta \approx 2.4$. This involves a pitchfork and a saddle-node bifurcation (see text). The HM and the MH states are stable in between two Hopf bifurcations located at $\theta \approx 3$ and $\theta \approx 16$, respectively. In panel (c) we show a two-dimensional diagram of the steady state value of A_1 varying $0 \leqslant \sigma \leqslant 1$ as a bifurcation parameter (for $\theta = 10$). The straight line is the continuation of the ZZ state; the folded line that of the LL state. The LL state has a limit point in which it connects with the MM state (i.e. a saddle-node bifucation) at $\sigma \approx 0.56$. The ZZ and the LL continuations cross in a transcritical bifurcation located at $\sigma \approx 0.1$. Here the two states switch stability and the LL state becomes unrealistic because of negative antibody populations. In panel (d) we show a two-dimensional diagram of the steady state value of A_1, varying $0 \leqslant \theta \leqslant 1\,000$ as a bifurcation parameter (for $\sigma = 1.48 \times 10^{-3}$). The straight line is the continuation of the ZZ state; the curved line that of the MM state. The ZZ and the MM continuations cross in a transcritical bifurcation located at $\theta \approx 675$. Here the two states switch stability and the MM state becomes unrealistic because of negative antibody populations. The two transcritical bifurcations in panels (c) and (d) correspond to $\sigma\theta = 1$ in Equation (40).

zero. [Note that the ZZ state also exists in the CABG model when $B_1 = B_2 = \sigma$, $A_1 = A_2 = 0$ and hence $f(A_1) = f(A_2) = 0$ and $\hat{A}_1 = \hat{A}_2 = G_1 = G_2 = 0$]. For our standard value of $\sigma = 1.48 \times 10^{-3}$ the LL state is negative in the AB model. However, Equation (40) predicts a bifurcation when $\sigma\theta = 1$. Indeed, for $\theta = 10$ Fig. 5c shows that the LL state becomes positive at a transcritical bifurcation at $\sigma \approx 0.1$, and for $\sigma = 1.48 \times 10^{-3}$ Fig. 5d shows another transcritical bifurcation around $\theta = 675$. (These bifurcation diagrams were done in the original coordinate system because $a = \ln 0$ is undefined.)

Figure 5c depicts the relationship between the two virgins states, ZZ and LL. The ZZ state is stable only when $\sigma < 0.1$. At $\sigma = 0.1$ there is an exchange of stability with the ZZ state becoming unstable and the LL state becoming stable. The light horizontal line is the continuation of the unstable ZZ state in which $B_1 = \sigma$ and $A_1 = 0$. The LL state is stable until it undergoes a saddle-node bifurcation at $\sigma \approx 0.56$. At this point the unstable MM state and the stable LL state unite and disappear. Summarizing, for $0 \leqslant \sigma < 0.1$ the ZZ state is the only stable virgin state, for $0.1 < \sigma < 0.56$ the LL state is the only stable virgin state and for $\sigma > 0.56$ the only virgin state is the unstable ZZ state. For our default value $\sigma = 1.48 \times 10^{-3}$ there is only one virgin state, the stable ZZ state. The unstable LL state is located at negative population values and is not physically realizable.

Figure 5d illustrates that we do not find the saddle-node bifurcation between the LL and MM state when θ is decreased. For $\sigma = 1.48 \times 10^{-3}$, i.e. for $\sigma\theta < 0.1$ [see Equation (40)], the LL is negative in the AB model (see Fig. 5c). This changes the S-shaped curve of the symmetric solutions in the B model into the parabola shown in Fig. 5b. Instead, as θ is increased the MM state and the ZZ state branches intersect at a transcritical bifurcation at an unrealistically high value of θ.

9.4. *Antibody lifetime, δ and μ.* Earlier work (De Boer and Hogeweg, 1989b; De Boer *et al.*, 1990) suggested that the oscillatory and chaotic behavior of the AB models depends on time scale differences between the B cell and antibody lifetimes. We therefore study the behavior of the basic AB model as a function of the parameters $\delta = d_A / d_B$ and $\mu = v d_C / d_B$.

First, if we set $\mu = 0$ and continue one of the immune states with δ as a bifurcation parameter we find a supercritical Hopf bifurcation at $\delta = 0.98$. This Hopf bifurcation forms the boundary between steady ($\delta > 0.98$) and oscillatory ($\delta < 0.98$) behavior of the model. Using this point as a starting point, we can continue the Hopf bifurcation as a function of the two antibody lifetime parameters δ and μ, and thus are able to map the parameter region where the immune states are stable—and where the principal behavior of the model is stationary—and the region where the immune states are unstable—and where the principal behavior turns out to be oscillations and/or chaos. The immune

states are stable in the shaded area in Fig. 6. The horizontal line in Fig. 6 corresponds to our estimate of the antibody turnover $\delta = 0.1$. As shown, for $\delta = 0.1$, the Hopf bifurcation is located at $\mu \approx 12.6$. Here, however, the Hopf bifurcation is numerically found to be subcritical.

In Fig. 6 the Hopf bifurcation switches from supercritical to subcritical around $\delta = 0.2$ (not shown). At a subcritical Hopf bifurcation an unstable limit cycle is born "backwards", surrounding the stable steady state, and hence local calculations around the steady state are not capable of predicting the attractor that is attained after the bifurcation. The attractor after such a "hard" bifurcation will lie far away (in phase space) from the steady state that loses stability and hysteresis should be expected close to the bifurcation in parameter space. The dynamic behavior in this region of parameter space will be explored in our companion paper, Part II.

Summarizing, for our estimates of realistic values of the ratio of B cell and antibody lifetime we expect the immune states, HM and MH, to be stable whenever μ is sufficiently large, i.e. roughly $\mu = vd_C/d_B > 10$. Using biological data we estimated that $\mu \approx 200$ and hence we predict that for immunologically realistic parameter values the immune states should be stable.

9.5. *The basic AB model without complex formation.* The basic AB model can be further simplified by ignoring complex formation, i.e. by setting $\mu = 0$. This enables us to pinpoint the effects of varying δ, the ratio of the antibody and B cell lifetimes. Figure 6 shows that for $\mu = 0$ a Hopf bifurcation is located at $\delta = 0.98$. Thus, for $\delta < 0.98$ all steady states except the virgin state are unstable.

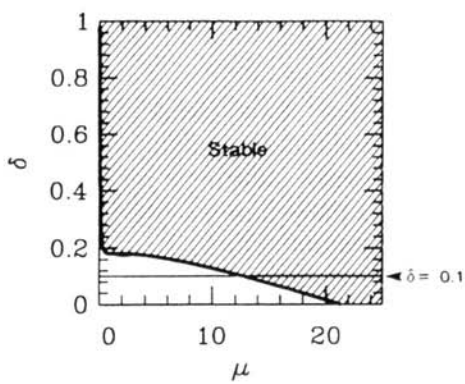

Figure 6. A two parameter diagram of the Hopf bifurcation of the immune states of the AB model varying μ and δ as bifurcation parameters. Parameters: $\theta = 10$, $\rho = 2$, $\sigma = 1.48 \times 10^{-3}$. We have shaded the region where the immune states are stable. The light horizontal line represents our estimate of the antibody lifetime $\delta = 0.1$. For $\mu = 0$ the Hopf bifurcation is located at $\delta \approx 0.98$ and is supercritical. For $d = 0.1$ the Hopf bifurcation is located at $\mu \approx 12.68$ and is subcritical. The Hopf switches from supercritical to subcritical around $\delta = 0.2$ (not shown).

We will restrict ourselves to the parameter region $0 < \delta \leqslant 1$, in which antibodies live longer than B cells. (Computations in the region $1 < \delta < 10^9$, for $\mu = 0, 0.1, 1, 10, \ldots, 10^4$, suggest that the immune states remain stable for larger values of δ.) We will discuss the behavior in this regime at length because the more realistic AB models have similar behavior, but are more difficult to explain.

An overview of the model's behavior is provided by Poincaré sections for different values of δ, see Fig. 7. The dots in Fig. 7 are values of a_d lying on the intersection of the limit cycles and the Poincaré plane $a_s = 0$. In the regions where no dots are plotted there does not appear to be any stable limit cycle behavior. The horizontal lines in Fig. 7 show the a_d value in the HM and MH state. These equilibrium a_d values are not sensitive to δ since they are located around $a_d \approx \ln \theta^{-1} \approx 4.6$ and around $a_d \approx \ln \theta^{-1} - \ln \theta \approx -4.6$.

The left half of Fig. 7, i.e. $0 < \delta < 0.43$, shows a limit cycle that in the projection of Fig. 8 circles both immune states crossing the plane $a_s = 0$ twice (see Figs 8a–d). For low values of δ the limit cycle is symmetric. A cycle is called symmetric when the two halves at each side of the lines of symmetry $a_d = 0$ and $b_d = 0$ are mirror images. Increasing δ decreases the limit cycle's amplitude, until the system goes through two pitchfork bifurcations at $\delta \approx 0.24$ and $\delta \approx 0.27$. In between these two symmetry breaking bifurcations we observe two

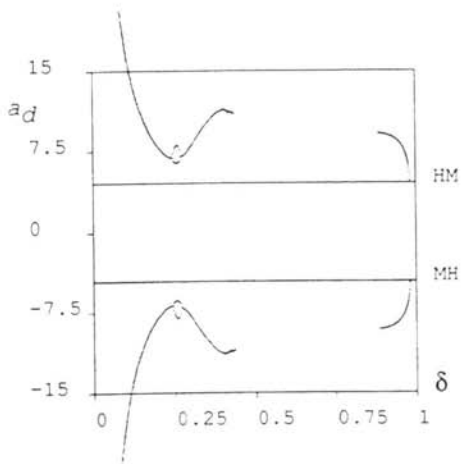

Figure 7. Partial bifurcation diagram of the AB model with respect to the parameter δ (the ratio of B cell and antibody lifetimes). Parameters: $0 \leqslant \delta \leqslant 1$, $\mu = 0$, $\theta = 10$, $\rho = 2$, $\sigma = 1.48 \times 10^{-3}$. The two horizontal lines show the equilibrium value of a_d in the two immune states as a function of δ. For each value of δ the dots are a_d values attained on limit cycle trajectories at a Poincaré section at the hyperplane $a_s = 0$. The limit cycles disappear at $\delta \approx 0.44$ and $\delta \approx 0.88$ where we find global bifurcations involving the invariant manifolds of the MM and HH states.

stable asymmetric oscillations (symmetric to each other) that each wind around both immune states, and each cross the plane $a_s = 0$ twice (see e.g. Figs 8a,b; $\delta = 0.25$). For $\delta > 0.27$, a symmetric limit cycle is again observed (see for example, Fig. 8c,d with $\delta = 0.4$), until it breaks into two stable asymmetric limit cycles at a pitchfork bifurcation for $\delta = 0.43$ (in Fig. 9a we plot one of the two). At approximately $\delta = 0.44$ the limit cycle disappears. In the range $0.44 \leqslant \delta \leqslant 0.88$ we have been unable to find any sustained time-dependent behavior and all trajectories that we have examined approach the virgin ZZ state.

The loss of the limit cycle at $\delta = 0.44$ appears to be associated with a global bifurcation involving the unstable manifold of the HH state, see Figs 9a,b. At $\delta = 0.43$ the outset of the HH state approaches the (asymmetric) limit cycle (we show only one branch of the outset in Fig. 9a). At $\delta = 0.44$, however, the HH outset approaches the virgin state (spiraling around the MM state). Here no limit cycle trajectories were found. Between $0.43 < \delta < 0.44$ we expect a heteroclinic connection between the HH and the MM state.

In the right part of Fig. 7 we can see, upon decreasing δ from one, that two asymmetric limit cycles are born at the supercritical Hopf bifurcation of the two immune states at $\delta = 0.98$. Each cycle winds around only one immune state and crosses the plane $a_s = 0$ only once (see Fig. 8e,f; $\delta = 0.95$). The unstable manifold of the HH state approaches the immune states above the Hopf at $\delta = 0.98$, and approaches the limit cycles below it. Decreasing δ the two limit cycles grow in amplitude until they apparently interact with the stable manifold of the MM state in between $0.88 < \delta < 0.89$. Here we expect another heteroclinic connection between the (one-dimensional) unstable manifold of the HH and the (one-dimensional) stable manifold of the MM state. At $\delta = 0.88$ the unstable manifold of the HH state asymptotically approaches the virgin ZZ state and the limit cycle is lost.

Summarizing, for $\mu = 0$ we find symmetric and asymmetric limit cycles in the regions where the immune states are unstable, i.e. for $\delta < 0.98$. The parameter range over which the model is capable of predicting oscillatory behavior is strongly dependent on global bifurcations involving the stable and unstable manifolds of the MM and the HH states, respectively. In the parameter region where the outset of the HH state approaches the ZZ state, the model seems unable to sustain oscillatory behavior. The possible complications involving the loss of these limit cycles have not been studied here. We only conclude that the limit cycles ultimately disppear around $\delta = 0.44$ and $\delta = 0.88$.

In Part II we will show that in more realistic versions of the AB model similar global bifurcations in the structure of the saddle invariant manifolds crucially affect the dynamic behavior of the model. Here, we would like to emphasize the similarity between the invariant manifold structure in Figs 4 and 9, i.e. between the B and the basic AB model.

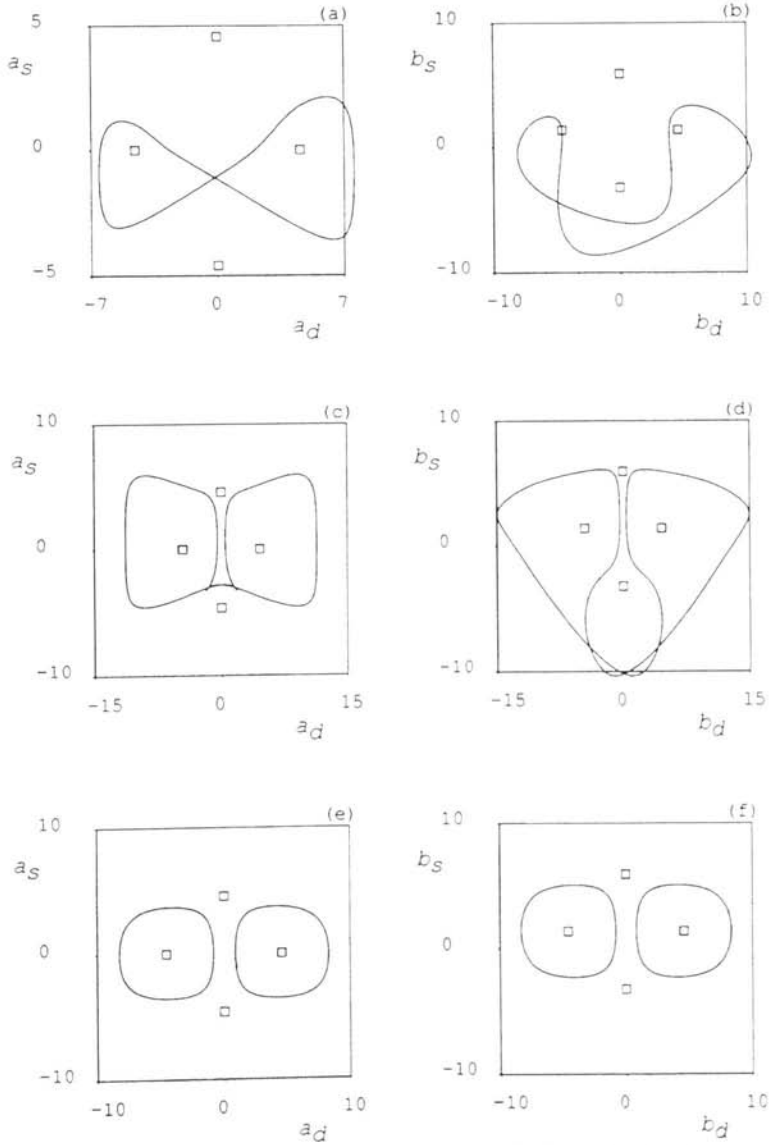

Figure 8. Representative shapes of the limit cycles found in the diagram of Fig. 7. The squares (□) show the location of the four activated equilibria. Panels (a), (c) and (e) show antibody concentrations, panels (b), (d) and (f) show B cell populations. (a) and (b) $\delta = 0.25$: we show one of the two asymmetric cycles found in the parameter interval between the two pitchfork bifurcations. (c) and (d) $\delta = 0.4$: a symmetric cycle winding around, in this projection, both immune states that crosses the plane $a_s = 0$ twice (counting crossings in one direction only). (c) and (f) $\delta = 0.95$: two symmetric cycles each winding around, in this projection, only one immune state.

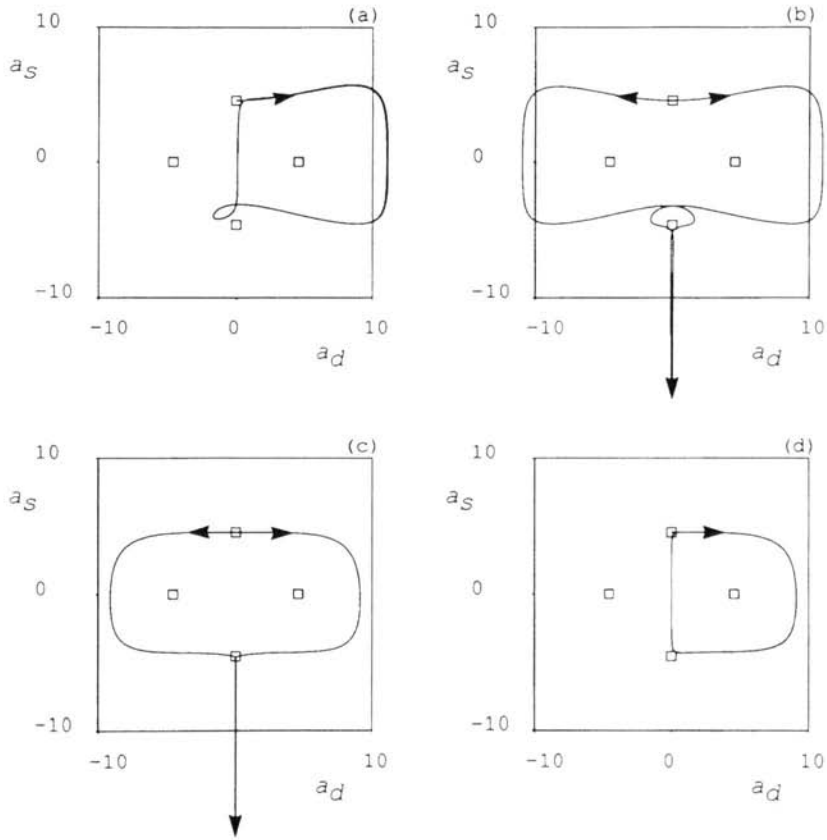

Figure 9. An illustration of the global bifurcations involved in the birth and death of the limit cycles of Fig. 7. We plot the unstable manifold of HH state of the basic AB model for four values of δ. Parameters: $\mu=0$, $\theta=10$, $\rho=2$, $\sigma=1.48\times10^{-3}$. (a) $\delta=0.43$: the manifold asymptotically approaches a stable asymmetric limit cycle surrounding one immune state. We show only one of the two sides of the manifold. (b) $\delta=0.44$: the manifold asymptotically approaches the ZZ state. (c) $\delta=0.88$: the manifold asymptotically approaches the ZZ state. (d) $\delta=0.89$: each side of the manifold asymptotically approaches one of the two stable limit cycles around the HM and MH states. At $\delta\approx0.98$ the HH states undergoes a Hopf-bifurcation and becomes stable. After this value the unstable manifold asymptotically approaches the asymmetric HM and MH states.

10. Discussion. In this paper we have modeled the idiotypic interaction between two B cells clones. Parts of the model have been analysed before (De Boer, 1988; De Boer and Hogeweg, 1989a,b; De Boer and Perelson, 1991; Segel and Perelson, 1989; Perelson and Weisbuch, 1992). We have estimated most of the parameters in the model and have introduced a new coordinate system that exploits the symmetry of the system. A detailed bifurcation analysis has provided insights into the relationships between the steady states and the

structure of their invariant manifolds. We have suggested that the global bifurcations associated with the stable and unstable manifolds associated with the HH and MM states bracket the parameter interval over which the oscillatory behavior is observed. Our companion paper, Part II, will demonstrate how crucial these global bifurcations in the invariant manifold structure are for understanding the complex (chaotic) dynamic behavior the model is capable of exhibiting.

The results shows that the immune states of the B model, that lacks antibodies, are typically stable and that the immune states of the basic AB model are typically unstable. The change in stability is caused by the difference in lifetime between the B cells and the antibodies. Here, the ratio of antibody and B cell turnover, δ, and the rate of complex removal, μ, determine the stability of the immune states. In Part II we will show that the other parameter determining the antibody lifetime, i.e. λ, the antibody residence time in the spleen, also determines the stability of the immune states.

Although our parameter choices are based on biological estimates, we have had to choose certain parameters carefully in order to be able to attain sustained idiotypic activation in the form of either non-virgin stationary states or oscillatory behavior. Thus, we have chosen the IgM affinity and secretion rate ($K = 10^6$/M and 10^4 molecules per sec) at the upper end of the feasible range. Additionally, we used a rather low estimate of the fluid volume of the spleen (i.e. 1% of the total volume). In the nondimensional model these parameter choices are reflected in choosing small values for α and β. Thus, relatively few B cells are required to attain the antibody concentration, $\sim (vK)^{-1}$, at which maximum cross-linking is achieved. For parameters of the non-dimensional model this choice is only reflected in σ. In other words, the virgin state is rather large in order to facilitate idiotypic activation.

Instead of using parameter values at the extremes of their feasible range, there are three modifications of the model that would also facilitate the attainment of significant IgM idiotypic interactions.

First, one may argue that B cells expressing IgM surface receptors are multireactive and that many clones will be involved in any idiotypic interaction. For example, Holmberg *et al.* (1989) review data showing that natural antibodies in newborn mice have a probability of over 20% of reacting with other IgM antibodies in the animal. This implies that the idiotype and anti-idiotype populations, B_1 and B_2, represent many clones rather than single clones. In terms of the model that would mean that the source of naive B cells from the bone marrow of any idiotype, σ, is much higher than we have assumed. Although this may be realistic, making σ high may eliminate the virgin state (see Fig. 4b). Sustained oscillatory and chaotic behavior would, however, remain feasible properties of the model. Memory, i.e. the switch from a virgin state to an immune state on antigen stimulation, would however be lost

as a model property if the virgin state disappeared. A model with a high value of σ might be most appropriate for the antibody dynamics during the development. Because a high value of σ eliminates the virgin state, the idiotypes are autonomously activated. This would correspond to the high connectivity of the immune network observed at birth. If one were to consider IgG antibodies rather than IgM, then affinities are typically much higher and sustained autonomous network behavior would be easy to obtain without raising σ. With low values of σ a virgin state exists. Thus, switches between virgin and immune states within a network might have to be mediated by IgG rather than IgM.

Second, one might question the symmetry of our phenomenological equation $f(h)$ for the cross-linking process. Models for receptor cross-linking have shown that the concentration of cross-linked receptors on the cell surface is a symmetric log bell-shaped function of the ligand concentrations, when the ligand is bivalent (Perelson and DeLisi, 1980). For multivalent ligands, such as the 10-valent IgM molecules that we consider here, cross-linking curves are asymmetric, with a slow rising part and a steep falling part (Perelson, 1981). In terms of B cell activation this means that B cells may become activated by extremely low concentrations of anti-idiotypic IgM. Since idiotypic activation is a self-reinforcing process, weak activation by low concentration may easily lead to full blown activation of idiotypic and anti-idiotypic B cells, with both classes of cells producing high IgM concentrations. In our phenomenological cross-linking function asymmetries can easily be incorporated by replacing the two saturation functions by Hill functions with different Hill coefficients.

Third, one may choose parameter values that correspond to lower affinities and lower secretion rates and conclude that idiotypic network interactions *per se* are not sufficient for maintaining stimulatory interactions and B cell proliferation. This opens the possibility that only those idiotypes that receive additional stimulation from, for instance, self antigens may be able to sustain network behavior with anti-idiotypes. Such an interpretation comes close to the hypothesis proposing that the immune network forms a central core of the immune system centered around self antigens (Vaz and Varela, 1978; Coutinho, 1989; Holmberg *et al.*, 1989). One can investigate this hypothesis in network models composed of many clones rather than just the two clones studied here. Such an analysis is quite feasible using the bitstring representation for antibodies (Farmer *et al.*, 1986; De Boer and Perelson, 1991) or shape space models (De Boer *et al.*, 1992b, 1992c; Segel and Perelson, 1988).

We thank Dr Mark A. Taylor for reading and commenting on the manuscript. This work was performed under the auspices of the U.S. Deparment of Energy. It was supported in part by NIH Grants AI28433 and RR06555 (A. P.), by NSF Grant CTS89-57213 (I. K.) and a Packard Foundation Fellowship (I. K.). It was also supported by the Santa Fe Institute through their

Theoretical Immunology Program and by the Los Alamos National Laboratory Center for Nonlinear Studies.

LITERATURE

Abramowitz, M. and I. A. Stegun. 1965. *Handbook of Mathematical Functions*, p. 17. NY: Dover.

Celada, F. 1971. The cellular basis of immunological memory. *Prog. Allergy* **15**, 223–267.

Coutinho, A. 1989. Beyond clonal selection and network. *Immunol. Rev.* **110**, 63–87.

Davies, K. A., V. Hird, S. Stewart, G. B. Sivolapenko, P. Jose, A. A. Epenetos and M. Walport. 1990. A study of *in vivo* complex formation and clearance in man. *J. Immunol.* **144**, 4613–4620.

De Boer, R. J. 1988. Symmetric idiotypic networks: connectance and switching, stability, and suppression. In: *Theoretical Immunology*. A. S. Perelson (Ed.), Part 2, pp. 265–289. SFI Studies in the Science of Complexity, Vol. III. Redwood City, CA: Addison–Wesley.

DeBoer, R. J. and P. Hogeweg. 1989a. Memory but no suppression in low-dimensional symmetric idiotypic networks. *Bull. math. Biol.* **51**, 223–246.

De Boer, R. J. and P. Hogeweg. 1989b. Unreasonable implications of reasonable idiotypic network assumptions. *Bull. math. Biol.* **51**, 381–408.

De Boer, R. J., I. G. Kevrekidis and A. S. Perelson. 1990. A simple idiotypic network model with complex dynamics. *Chem. Engng Sci.* **45**, 2375–2382.

De Boer, R. J., I. G. Kevrekidis and A. S. Perelson. 1993. Immune network behavior—II. From oscillations to chaos and stationary states. *Bull. math. Biol.* **55**, 781–816.

De Boer, R. J., A. U. Neumann, A. S. Perelson, L. A. Segel and G. Weisbuch. 1992a. Recent approaches to immune networks. In: *Proc. First European Biomathematics Conference*. V. Capasso and P. Demongeot (Ed.). Berlin: Springer-Verlag, in press.

De Boer, R. J., J. D. van der Laan and P. Hogeweg. 1992b. Randomness and pattern scale in the immune network: a cellular automaton approach. In: *Thinking about Biology*. W. D. Stein and F. J. Varela (Ed.), Part 2, SFI Studies in the Science of Complexity, Vol. III. Redwood City, CA: Addison-Wesley, in press.

De Boer, R. J., L. A. Segel and A. S. Perelson. 1992c. Pattern formation in one and two-dimensional shape space models of the immune system. *J. theor. Biol.* **155**, 295–233.

De Boer, R. J. and A. S. Perelson. 1991. Size and connectivity as emergent properties of a developing immune network. *J. theor. Biol.* **149**, 381–424.

Dibrov, B. F., M. A. Livshits, and M. V. Volkenstein. 1977. Mathematical model of immune responses. *J. theor. Biol.* **65**, 609–631.

Farmer, J. D., N. H. Packard and A. S. Perelson. 1986. The immune system, adaptation, and machine learning. *Physica* **22D**, 187–204.

Fowler, A. C. 1981. Approximate solution of a model of biological immune responses incorporating delay. *J. math. Biol.* **13**, 23–45.

Hoffmann, G. W. 1975. A theory of regulation and self–nonself discrimination in an immune network. *Eur. J. Immunol.* **5**, 638–647.

Holmberg, D., A. Andersson, L. Carlson and S. Forsgen. 1989. Establishment and functional implications of B-cell connectivity. *Immunol. Rev.* **110**, 89–103.

Hooijkaas, H., R. Benner, J. R. Pleasants and B. S. Wostmann. 1984. Isotypes and specificities of immunoglobulins produced by germ-free mice fed chemically defined ultrafiltered "antigen-free" diet. *Eur. J. Immunol.* **14**, 1127–1130.

Jerne, N. K. 1974. Towards a network theory of the immune system. *Ann. Immunol. (Inst. Pasteur)* **125 C**, 373–389.

Landis, E. M. and J. R. Pappenheimer. 1962. Exchange of substances through the capillary walls. In: *Handbook of Physiology. Circulation II*. Washington, DC: American Physiology Society.

Lundkvist, I., A. Coutinho, F. Varela and D. Holmberg. 1989. Evidence for a functional idiotypic network amongst natural antibodies in normal mice. *Proc. Natn. Acad. Sci. USA* **86**, 5074–5078.

Pabst, R. 1988. The role of the spleen in lymphocyte migration. In: *Migration and Homing of Lymphoid Cells*. A. J. Husband (Ed.), Vol. I, pp. 63–84. Boca Raton, FL: CRC Press.

Pereira, P., L. Forni, E. L. Larsson, M. Cooper, C. Heusser and A. Coutinho. 1986. Autonomous activation of B and T cells in antigen-free mice. *Eur. J. Immunol.* **16**, 685–688.

Perelson, A. S. 1981. Receptor clustering on a cell surface. III. Theory of receptor cross-linking by multivalent ligands: Description by ligand states. *Math. Biosci.* **53**, 1–39.

Perelson, A. S. 1984. Some mathematical models of receptor clustering by multivalent antigens. In: *Cell Surface Dynamics: Concepts and Models*. A. S. Perelson, C. DeLisi and F. W. Wiegel (Eds), pp. 223–276. Marcel Dekker: New York.

Perelson, A. S. 1988. *Theoretical Immunology*. A. S. Perelson (Ed.), Part 2, SFI Studies in the Science of Complexity, Vol. III. Redwood City, CA: Addison–Wesley.

Perelson, A. S. 1989. Immune network theory. *Immunol. Rev.* **110**, 5–36.

Perelson, A. S. and C. DeLisi. 1980. Receptor clustering on a cell surface. I. Theory of receptor cross-linking by ligands bearing two chemically identical functional groups. *Math. Biosci.* **48**, 71–110.

Perelson, A. S. and G. Weisbuch. 1992. Modeling immune reactivity in secondary lymphoid organs. *Bull. math. Biol.* **54**, 649–672.

Richter, P. H. 1975. A network theory of the immune system. *Eur. J. Immunol.* **5**, 350–354.

Richter, P. H. 1978. The network idea and the immune response. In: *Theoretical Immunology*. G. I. Bell, A. S. Perelson and G. H. Pimbley Jr (Eds). New York: Marcel Dekker.

Segel, L. A. and A. S. Perelson. 1988. Computations in shape space. A new approach to immune network theory. In: *Theoretical Immunology*. A. S. Perelson (Ed.), Part 1, pp. 349–382, SFI Studies in the Sciences of Complexity. Redwood City, CA: Addison–Wesley.

Segel, L. A. and A. S. Perelson. 1989. Shape space analysis of immune networks. In: *Cell to Cell Signalling: From Experiments to Theoretical Models*. A. Goldbeter (Ed.), pp. 273–283. New York: Academic Press.

Segel, L. A. and A. S. Perelson. 1991. Exploiting the diversity of time scales in the immune system: A B-cell antibody model. *J. statisc. Phys.* **63**, 1113–1131.

Sprent, J. 1989. T lymphocytes and the thymus. In: *Fundamental Immunology*. W. E. Paul (Ed.), pp. 69–93. New York: Raven Press.

Stewart, J. and F. J. Varela. 1989. Exploring the meaning of connectivity in the immune network. *Immunol. Rev.* **110**, 37–61.

Stewart, J. and F. J. Varela. 1990. Dynamics of a class of immune networks. II. Oscillatory activity of cellular and humoral components. *J. theor. Biol.* **144**, 103–115.

Strand, F. L. 1978. *Physiology*, p. 559. New York: Macmillan.

Varela, F. J. and A. Coutinho. 1991. Second generation immune networks. *Immunol. Today* **12**, 159–166.

Varela, F. J., A. Anderson, G. Dietrich, A. Sundblad, D. Holmberg, M. Kazatchkine and A. Coutinho. 1991. The population dynamics of natural antibodies in normal and autoimmune individuals. *Proc. Natn. Acad. Sci. USA* **88**, 5917–5921.

Vaz, N. N. and F. J. Varela. 1978. Self and non-sense: an organism-centered approach to immunology. *Med Hypoth.* **4**, 231–267.

Weisbuch, G., R. J. De Boer and A. S. Perelson. 1990. Localized memories in idiotypic networks. *J. theor. Biol.* **146**, 483–499.

Weiss, L. (1972). *The Cells and Tissues of the Immune System*. Englewood Cliffs, NJ: Prentice-Hall.

Received 4 May 1992
Revised 20 August 1992